Wind Project Data Management Plan

Lynn B. Wilson III
NASA GSFC
Project Scientist
August 15, 2024

Table of Contents

1 The *Wind* Mission **2**
1.1 Spacecraft Health . . . 3
1.2 Instrument Status . . . 5
1.3 Science Team . . . 8
1.4 Mission Team . . . 9
2 Instrument Descriptions **10**
2.1 MFI Instrument . . . 10
2.2 3DP Instrument . . . 11
2.3 WAVES Instrument . . . 14
2.4 SWE Instrument . . . 16
2.5 SMS Instrument . . . 18
2.6 EPACT Instrument . . . 22
2.7 KONUS Instrument . . . 25
2.8 TGRS Instrument . . . 26
3 Ground Operations **27**
3.1 Data Flow . . . 28
4 Data Products **30**
4.1 SWE Ions . . . 31
4.2 SWE Electrons . . . 33
4.3 3DP . . . 34
4.4 SMS . . . 36
4.5 EPACT . . . 38
4.6 MFI . . . 40
4.7 WAVES . . . 41
4.8 KONUS and TGRS . . . 43
5 Data Usage Summary Instructions **44**
5.1 Pre-calibrated Science Quality Data Sets . . . 44
5.1.1 Quasi-static Magnetic Fields . . . 44
5.1.2 Number Density Calibration . . . 45
5.1.3 Thermal Particle Data . . . 46
5.1.4 Suprathermal Particle Data . . . 48
5.1.5 High Frequency Electromagnetic Fields . . . 50
5.1.6 3DP lz Data Analysis . . . 51
Definitions and Notation **52**
Acronyms and Initialisms **53**
References **59**

1 The *Wind* Mission

Much of the following is taken directly or adapted from *Wilson III et al.* [2021a].

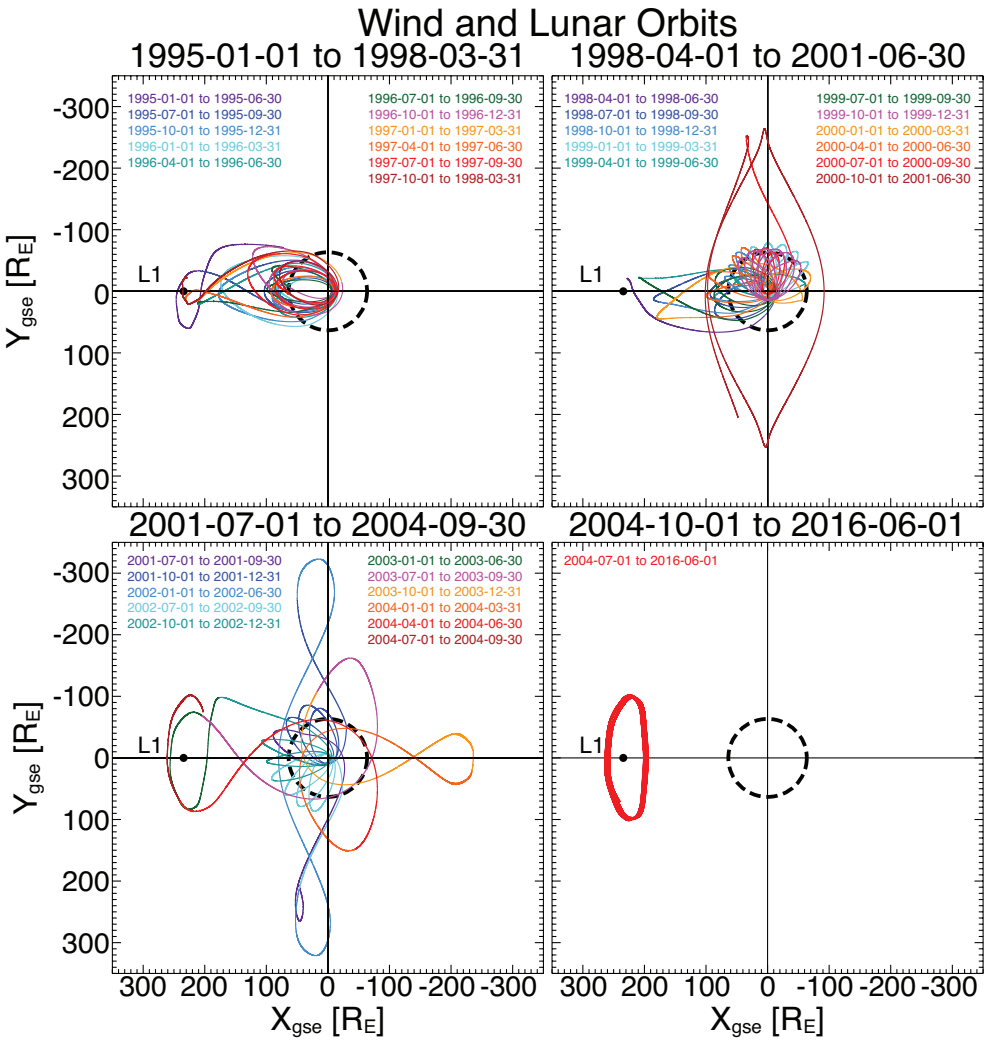

Figure 1: *Orbital trajectories of the* Wind *spacecraft in the GSE XY plane from 1 November 1994 to 1 June 2016. Colors denote time ranges as indicated. The dashed black circle indicates the Moon's orbit [Adapted from Figure 1 in Wilson III et al., 2021a]. Note that the orbit has not noticeably changed since 1 June 2016.*

NASA launched the *Wind* spacecraft on November 1, 1994. *Wind* and *Polar* [*Harten and Clark*, 1995] were part of the stand-alone Global Geospace Science (GGS) Program [*Acuña et al.*, 1995], a subset of the International Solar Terrestrial Physics (ISTP) Program [*Whipple and Lancaster*, 1995]. The ISTP Program included the additional missions *Geotail* [*Nishida*, 1994], the SOlar and Heliospheric Observatory or *SoHO* [*Domingo et al.*, 1995], and *Cluster* [*Escoubet et al.*, 1997]. The objective of the ISTP program was to study the origin of solar variability and activity, the transport of manifestations of that activity to the Earth via plasma processes, and the cause-and-effect relationships between that time varying energy transport and the near-earth environment.

Wind is a spin stabilized spacecraft – spin axis aligned with ecliptic south – with a spin period of ∼3 seconds. Prior to May 2004, *Wind* performed a series of orbital maneuvers *Franz et al.* [1998], as shown in Figure 1, that led to the spacecraft visiting numerous regions of the near-Earth enviroment. For instance, between launch and late 2002 *Wind* completed ∼67 petal orbits through

the magnetosphere and two lunar rolls out of the ecliptic in April and May of 1999. Between August 2000 and June 2002 *Wind* completed four east-west prograde 1:3–Lissajous orbits reaching $\gtrsim$300 R_E along the ±Y-GSE direction *Fränz and Harper* [2002]. From November 2003 to February 2004 *Wind* performed an excursion to the second Earth-Sun libration point, or Lagrange point, called L2[1].

During the magnetosphere passes, *Wind* also made several lunar flybys. *Wind* completed 10 wake crossings before entering a Lissajous orbit at L1 in 2004. Table 1 lists all crossings of the lunar optical wake *Ogilvie and Desch* [1997].

Table 1: Optical Lunar Wake Transits by *Wind*

Start time [UTC]	End time [UTC]
1994-12-01/15:04:07	1994-12-01/15:29:10
1994-12-27/14:36:30	1994-12-27/15:22:36
1996-03-24/05:19:43	1996-03-24/06:24:50
1996-11-13/01:43:16	1996-11-13/03:07:25
1999-04-01/20:38:02	1999-04-01/20:53:04
1999-05-12/20:52:12	1999-05-12/21:04:14
2000-08-19/15:35:45	2000-08-19/16:51:53
2001-12-05/16:48:53	2001-12-05/17:54:00
2002-07-18/17:46:39	2002-07-18/18:42:45
2002-11-30/11:30:28	2002-11-30/12:16:33

In May 2004, *Wind* made its final major orbital maneuver using a lunar gravitational assist to insert it into a Lissajous orbit about the first Earth-Sun libration point, labeled L1 by late June 2004. Note that *Wind*'s L1 orbit has a ±Y-GSE(±X-GSE) displacement about the sun-Earth line of ∼100 R_E(∼35 R_E), much larger than the other NASA mission at L1, ACE. Note that the ±Z-GSE displacement from the ecliptic plane is $\lesssim$30 R_E for both ACE and *Wind*. On June 26, 2020, the *Wind* flight operations team (FOT) successfully completed the first halo orbit insertion maneuver and the second was successfully completed on August 31, 2020. The third maneuver was successfully completed on November 9, 2020. This orbital change was necessary to prevent the spacecraft trajectory from entering the solar exclusion zone – around the solar disk where solar radio emissions cause sufficient interference with spacecraft communications to prevent telemetry signal locks. The projection of the orbit in the ecliptic plane will not noticeably change, however the out-of-ecliptic projection will now be a stationary ellipse centered on the solar disk.

1.1 Spacecraft Health

Wind continues to operate in good health. The communication system was successfully reconfigured in 2000 to enhance the telemetry margins and reliance on a single digital tape recorder (with two tape units) since 1997 has never hindered operations. The flight operations team (FOT) took steps to minimize wear and extend the lifespan of the two tape units. Since the last Senior Review, the spacecraft has experienced the usual instrument latch-ups and single-event upsets (SEUs) that are likely caused by high energy particles. As in the past, the FOT was able to restore all instruments to fully operational within a day or two depending on Deep Space Network (DSN) scheduling. The automation of the recovery process for the WAVES instrument after latch-ups (i.e., due to SEUs) was successfully completed in October 2016 and the spacecraft command tables

[1]Note that L2 is located ∼233–235 R_E downstream of Earth and ∼500 R_E downstream of the Advanced Composition Explorer (ACE) *Stone et al.* [1998]. For reference, ACE launched in 1997 and was designed to study energetic particles and their composition. Unlike *Wind*, ACE was not designed to study kinetic physics or remote solar and astrophysical phenomena using electric fields.

now include automated tests of the SWE electron instrument. Thus, *Wind* continues to maintain a fully operational status.

On Oct. 27, 2014 at 21:59:38 GMT, the *Wind* command and attitude processor (CAP) suffered two simultaneous SEUs. The redundant nature of the *Wind* spacecraft bus allowed the FOT to successfully switch to a second CAP, CAP2. The FOT began the recovery of CAP1 on Jan. 21, 2015 and finished Jan. 30, 2015, and the spacecraft was fully recovered at ∼17:50 UTC on Jan. 30, 2015.

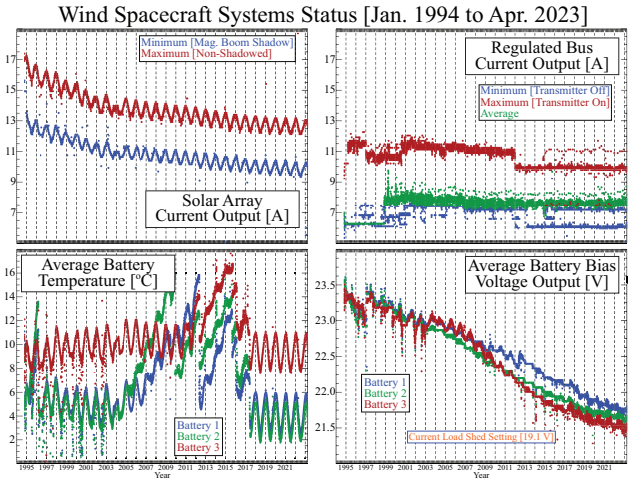

Figure 2: ***Summary of* Wind*'s Power System Status:*** *The* Wind *spacecraft systems status plotted from Jan. 1, 1994 to Apr. 1, 2023 as daily averages.*

The CAP1 anomaly resulted in a complete loss of data from October 27, 2014 until November 7, 2014 (i.e., 11 days or ∼3% annual total) and partial loss from all instruments between November 7–20, 2014 (i.e., 14 days or ∼4% annual total). The SWE instrument suffered complete data loss between October 27, 2014 and November 26, 2014 (i.e., 30 days or ∼8% annual total) and partial loss (HK only) from October 27, 2014 to December 1, 2014 (i.e., 35 days or ∼10% annual total). During the recovery process between Jan. 28–30, 2015 while CAP1 was in control, the attitude/telemetry information was invalid for ∼4 hrs 41 mins (i.e., <5% of those four days).

On April 11, 2016 one of the two tape units (TUA) began experiencing issues related to the read/write head causing ∼few percent data loss per day. The flight operations team successfully switched the primary record unit to TUB on May 6, 2016 to extend the life of TUA and reduce data loss. TUB is fully operational and averages >98.5% data recovery rates.

An examination of the spacecraft power systems (see Figure 2) shows that the batteries can maintain average bias voltages high enough to exceed the current load shed setting of 19.1 V until at least mid-2056 based on an extrapolation beyond the date range of the lower right panel. To cause a spacecraft reset, all three batteries must simultaneously fall below this load shedding voltage level which is commandable from the ground and will be changed when necessary to avoid a spacecraft reset. The load shedding can be safely reduced to at least 18.2 V (reached at least 20 years beyond 2056 based on present trends).

All three batteries went through mode changes prior to 2020 to reduce the maximum charge voltage. Each battery was experiencing excess charging, causing an increase in temperature (see lower-left-hand panel in Figure 2) and reduction in efficiency. The mode changes successfully reduced the temperatures to nominal ranges. The current trend shows that the battery temperatures will not exceed the critical threshold of ∼17°C until well after the year ∼2100.

The solar array output is producing more than enough current for spacecraft operations and will continue to do into early ∼2044, assuming that the maximum current drawn from the batteries (i.e., red line in upper right in Figure 2) does not exceed the average solar array output (not shown). The maximum solar array output (i.e., red line in upper left-hand panel) will not drop to the maximum regulated bus output until mid ∼2058, assuming current trends hold. Therefore, *Wind* can operate at current capacity for the next several decades.

Wind continues to maintain a large fuel reserve. As of August 7, 2024, the tanks contained ∼34.9 kg of fuel, which is equivalent to ∼70 m/s of radial delta-V assuming normal thruster operations. Typically only four station keeping maneuvers are performed each year, each requiring only ∼0.12 kg of fuel. Thus, *Wind* has enough fuel for ∼70 years.

1.2 Instrument Status

The *Wind* instrument names and acronyms are listed below in Table 2.

Table 2: *Wind* Instrument Names

Abbrev.	Instrument name	Reference
TGRS	Transient Gamma-Ray Spectrometer	*Owens et al.* [1995]
KONUS	Gamma-Ray Spectrometer	*Aptekar et al.* [1995]
EPACT	Energetic Particles: Acceleration, Composition, and Transport	*von Rosenvinge et al.* [1995a]
SMS	Solar Wind and Suprathermal Ion Composition Experiment	*Gloeckler et al.* [1995]
MFI	Magnetic Field Investigation	*Lepping et al.* [1995]
WAVES	The Radio and Plasma Wave Investigation	*Bougeret et al.* [1995]
3DP	Three-Dimensional Plasma and Energetic Particle Investigation	*Lin et al.* [1995]
SWE	Solar Wind Experiment	*Ogilvie et al.* [1995]

It is important to note that unlike most other missions, *Wind* was designed with significant redundancy in its measurements. For instance, there are at least five possible measurements of the solar wind number density (two from 3DP, two from SWE, one from WAVES, and one from SMS under certain conditions) and prior to 2000 there were two different gamma ray instruments. The MFI comprises two fluxgate magnetometers at different locations on a 12 meter boom (one closer at ∼8 m, the other at 12 m) which improves spacecraft noise/artifact removal. There are three separate measurements of protons with energies >50 keV (one from 3DP, one from SMS, and one from EPACT). Finally, there are at least three separate measurements of heavy ions (i.e., ions more massive than alpha-particles).

Seven of the eight *Wind* instruments, including all of the fields and particles suites, remain largely or fully functional. The only instrument fully turned off is the TGRS γ-ray instrument that was designed for only a few years of operations (instrument off prior to ∼January 2000). Aside from temporary data losses due to a command and attitude processor (CAP) and tape unit anomaly (both issues were resolved or mitigated, discussed in detail below), the instruments continue to return >98% of all captured data annually. The dates of significant spacecraft and instrumental issues are listed in Table 3 for reference.

The instrument capabilities and current status are shown in Table 4 (see the Glossary and Acronyms Appendices for definitions). Below we discuss the instrument anomalies in more detail.

The EPACT APE-A/APE-B/IT high voltage power supply (HVPS) suffered a loss of gain in October 1995. The EPACT-APE detector only returns two energy channels of ∼5 and ∼20 MeV protons during enhanced periods. The EPACT-LEMT and -STEP telescopes continue to operate normally, providing crucial and unique observations of solar energetic particles up to 10 MeV in energy. The SMS-SWICS solar wind composition sensor had to be turned off in May 2000. The SMS DPU experienced a latch-up reset on 26 June 2009 causing the MASS acceleration/deceleration power supply to stay in a fixed voltage mode, rather than stepping through a set of voltages. The moderate risk of power cycling of the SMS DPU required to fix this issue was declined to protect the unique and fully functional SMS-STICS sensor. In 2010, MASS experienced a small degradation in the acceleration/deceleration power supply further reducing the instrument efficiency. However, the SMS-MASS sensor still returns science quality data.

The VEIS thermal electron detectors on the SWE instrument suffered high voltage power sup-

Table 3: Wind Instrument and Spacecraft Anomalies

Date	**Part Affected**	**Impact**
January 19, 1995	GTM1[a]	failure
October 1995	APE-A/APE-B/IT HVPS[b]	suffered a loss of gain
April 30, 1997	CAP1[c]	Reed-Solomon encoder failure
December 13, 1997	DTR2[d]	power supply failure
January 2000	TGRS	γ-ray instrument turned off (planned coolant outage)
May 2000	SMS-SWICS	solar wind composition sensor turned off
June 2001	SWE-VEIS	thermal electron detectors HVPS failure
August 2002	SWE-Strahl	reconfigured to recover VEIS functionality
June 2009	SMS DPU	experienced a latch-up reset – MASS acceleration/deceleration power supply in fixed voltage mode
2010	SMS-MASS	experienced a small degradation in the acceleration/deceleration power supply
May 19, 2014	3DP-PESA Low	suffered an anomaly that affected only the telemetry HK[e] data
October 27, 2014	CAP1	anomaly at ~21:59:38 GMT
November 7, 2014	CAP2	set to primary while recovery starts on CAP1
November 26, 2014	SWE	full reset due to CAP1 anomaly
January 30, 2015	CAP1	fully recovered
April 11, 2016	DTR1 TUA	began experiencing read/write errors (~1% bit errors)
May 6, 2016	DTR1 TUB	FOT sets as primary recorder

[a] two GGS telemetry modules, GTM1 and GTM2 [b] high voltage power supply
[c] two command and attitude processors, CAP1 and CAP2 [d] two digital tape recorders, DTR1 and DTR2, each with independent tape units, TUA and TUB [e] house keeping

ply problems in June 2001. In August 2002 the SWE Strahl sensor was reconfigured to recover most of the original functions. Moreover, the 3DP instrument also covers the impacted electron measurements making these observations still redundant and hence robust. The entire SWE instrument suite required a full reset due to the CAP anomaly (see Section 1.1 for details), which resulted in a complete loss of data from late Oct. 27, 2014 to Nov. 26, 2014, and partial loss until Dec. 1, 2014 when the instrument was returned to nominal operations.

On May 2014 the 3DP instrument (specifically PESA Low) suffered an anomaly that only affected the telemetry house keeping (HK) data. A quick investigation showed that while the telemetry information (e.g., micro-channel plate grid voltage) showed unreliable instrument operations information, the science data remained unaffected (i.e., no noticeable change in flux was observed during and after event). All the other detectors within the 3DP instrument suite continue to operate nominally. Thus, the anomaly resulted in no loss of scientific data.

Table 4: Operational Instruments on *Wind*

Name	Type	Cadence	Range	Status & Notes
MFI				**Nominal**
	3 $B_{o,j}$[a]	∼11–22 sps[b]	±4 – ±65,536 nT	±0.001 – ±16 nT
WAVES				**Nominal**
TDS Fast	2 δE_j	1.8–120 ksps	∼0.1–300 mV/m	∼80 μV rms
TDS Slow	1 or 3 δE_j	0.1–7.5 ksps	∼0.5–300 mV/m	∼300 μV rms
	1 or 3 δB_j	0.1–7.5 ksps	∼0.25 – $\gtrsim$30 nT	$\sim 10^{-9}$ nT^2 Hz^{-1} @ 100 Hz
TNR	1 δE_j	∼1 min	∼4–256 kHz	∼7 nV Hz$^{-1/2}$
RAD1	2 δE_j	∼1 min	∼20–1040 kHz	∼7 nV Hz$^{-1/2}$
RAD2	2 δE_j	∼1 min	∼1.1–14 MHz	∼7 nV Hz$^{-1/2}$
3DP				**Nominal**
EESA	e^-	∼3–22 s	∼0.003–30 keV	∼20% $\Delta E/E$[c], ∼5.6–22.5°
PESA	H^+, He^{2+}	∼3–75 s	∼0.003–30 keV	∼20% $\Delta E/E$, ∼5.6–22.5°
SST Foil	e^-	∼12 s	∼25–400 keV	∼30% $\Delta E/E$, $\gtrsim$22.5°
SST Open	H^+	∼12 s	∼25–6000 keV	∼30% $\Delta E/E$, $\gtrsim$22.5°
SWE				**VEIS Off**, **Strahl Reconf.**
FCs	H^+, He^{2+}	∼92 s	∼0.15–8 keV	∼6.5% $\Delta E/E$
Strahl	e^-	∼12 s	∼0.005–5 keV	∼3% $\Delta E/E$ ∼3° × 30°
SMS				**SWICS Off**, **MASS Reduced**
STICS	H – Fe	$\gtrsim$3 min	∼8–226 keV/e 1–60 amu/e	∼5% $\Delta E/E$, ∼4° × 150° ∼12% $\Delta M/M$[d]
EPACT				**IT off**, **APE Reduced**
LEMT	He – Fe	$\gtrsim$5–60 min	∼2–12 MeV/n ∼2–90 Z	$\gtrsim$20% $\Delta E/E$ $\gtrsim$2% $\Delta Q/Q$[e]
STEP	H – Fe	$\gtrsim$10 min	∼0.02–2.56 MeV/n	$\gtrsim$30% $\Delta E/E$ ∼17° × 44°
KONUS	photons	$\gtrsim$2 ms $\gtrsim$3 s	∼0.02–15 MeV ∼0.02–1.5 MeV	**Nominal** $\gtrsim$5% $\Delta E/E$ Background Mode
TGRS	photons	$\gtrsim$62 μs	∼0.025–8.2 MeV	**Off (out of coolant)** ∼3 keV @ 1 MeV eff. ∼43% @ 511 keV

[a] three magnetic field vector components [b] samples per second [c] normalized energy resolution
[d] normalized mass resolution [e] normalized charge resolution

1.3 Science Team

The *Wind* instrument/science team is a small but dedicated group of scientists. Due to the longevity of the mission, a number of the original instrument PIs have retired or passed away. The SWE instrument suite is currently headed by **Bennett A. Maruca (University of Delaware)** with Michael L. Stevens (Harvard Smithsonian) leading the SWE Faraday Cup team. **Stuart D. Bale (University of California, Berkeley SSL)** is the PI of 3DP. **Andriy Koval (University of Maryland, Baltimore County/Code 672)** took over as PI of the MFI instrument replacing Adam Szabo (GSFC), who moved on to other missions. **Susan T. Lepri (University of Michigan, Ann Arbor)** is the PI for SMS. **Keith Goetz (University of Minnesota, Twin Cities)** is the American PI for WAVES while the French PI is **Karine Issautier (Observatoire de Paris-Meudon)**[2]. Both the original and previous acting EPACT PIs, Tycho von Rosenvinge and Allen Tylka, respectively, retired so **Ian G. Richardson (University of Maryland, College Park/Code 672)** took over as the EPACT PI in late 2019. Finally, unfortunately Rafail Aptekar passed away in late December 2020 so **Dmitry Frederiks (Ioffe Institute, Laboratory for Experimental Astrophysics, St. Petersburg, Russia)** has taken over as the KONUS PI. Lynn B. Wilson III has been Project Scientist for *Wind* since June 2016. A summary of the instrument leads can be found in Table 5.

Table 5: The status of the *Wind* instruments

Instrument	Principal Investigator	Institution	Status
SWE	B.A. Maruca	Electrons: GSFC, UNH Ions: SAO	Strahl detector reconfigured Faraday Cup fully operational
3DP	S.D. Bale	UC Berkeley	Fully operational
MFI	A. Koval	GSFC/UMBC	Fully operational
SMS	S. Lepri	U. Michigan	SWICS turned off MASS reduced coverage STICS fully operational
EPACT	I. Richardson	GSFC/UMCP	IT turned off APE – only 5 and 20 MeV protons LEMT and STEP operational
WAVES	K. Goetz	U Minnesota	Fully operational
KONUS	D. Frederiks	Ioffe Institute, Russia	Fully operational
TGRS	B. Teegarden	GSFC	Intentionally turned off (ran out of coolant)

[2]The original PI was Jean Louis Bougeret of France, with a strong partnership between the French institutions and the University of Minnesota and NASA Goddard Space Flight Center. The previous American PIs were Michael Kaiser and Robert MacDowall (both at GSFC).

1.4 Mission Team

The current *Wind* mission management team is as follows. Lynn B. Wilson III (GSFC, Code 672) is the Project Scientist. Patrick Koehn (NASA HQ) is the Program Scientist. Robert F. Stone (GSFC, Code 584) is the Mission Director and Rich Burns (GSFC, Code 444) is the Program Manager. The flight operations team (FOT) is headed by Jacqueline M. Snell (GSFC/KBRwyle, Code 444) and the lead engineer is Eric S. Smith (GSFC/KBRwyle, Code 444).

2 Instrument Descriptions

This section discusses some more specific details of the physical specifications and measurements made by the *Wind* instruments.

2.1 MFI Instrument

The *Wind* MFI instrument consists of a dual, triaxial fluxgate magnetometer mounted on a ∼12 m deployable boom [*Lepping et al.*, 1995]. The outer sensor is mounted at the end of the boom while the inner at ∼2/3 of the length of the boom. The detector has eight dynamic ranges[3] from ±4 nT to ±65,536 nT using a 12-bit analog-to-digital-convert (ADC) corresponding to eight digital resolutions[4] varying from ±0.001 nT to ±16 nT. The sensor noise level is nominally $\lesssim$0.006 nT rms over ∼0–10 Hz. This results in a precision of ∼0.025% and a sensitivity of ∼0.008 nT/step quantization. The instrument returns one 3-vector magnetic field ∼10.9 times per second for most of the mission[5]. The onboard sun sensor and star trackers allow the instrument team to correctly calculate the spin phase of the spacecraft when in Earth's (or the Moon's) shadow throughout the early phase of the mission (i.e., prior to ∼May 2004). This is critical for properly calculating the magnetic field in these regions. The instrument also suffers from several extra harmonics above the expected spin tone harmonics due to power switching between the solar arrays and batteries turning on and off during rotation[6] [e.g., *Koval and Szabo*, 2013]. These are now removed through several automated processes but the user is still warned to be careful with data near the Nyquist frequency of the instrument.

[3] i.e., ±4 nT, ±16 nT, ±64 nT, ±256 nT, ±1024 nT, ±4096 nT, ±16,384 nT, and ±65,536 nT

[4] i.e., ±0.001 nT, ±0.004 nT, ±0.016 nT, ±0.0625 nT, ±0.25 nT, ±1.0 nT, ±4.0 nT, and ±16 nT

[5] That is, after ∼October 1997 the highest sample rate was ∼10.9 sps whereas before ∼November 1997 there were periods with ∼22 sps.

[6] There is also an issue of a ballast mass (copper plate placed outside thermal blankets) being installed near the end of the magnetometer boom shortly before launch that causes time-varying magnetic field signatures due to variation in exposure to sunlight and its rotation through a magnetic field. This is why the instrument team relies primarily upon the inner than outer magnetometer. Note that the MFI team did not find out about the addition until after launch when examining pre-launch photographs.

2.2 3DP Instrument

Physical Specs: The *Wind* 3DP instrument [*Lin et al.*, 1995] is comprised of four electrostatic analyzers (ESAs) and three arrays of double-ended semi-conductor solid state telescopes (SSTs). Below we describe the generic properties/parameters of each instrument type and then list the specific specs of each detector. Details come from the original instrument paper by *Lin et al.* [1995] and in-person (and/or email) discussions with Davin E. Larson, James (Jim) McFadden, and Robert (Bob) Lin.

The ESAs are spherical top-hat analyzers on top of microchannel plates (MCPs) that sit above anodes which measure current pulses generated by electron showers emitted from the MCPs. The ESAs are split into low (L) and high (H) energy ranges[7] and into electron (E) and ion (P) detectors. They are thus named EESA Low, EESA High, PESA Low, and PESA High. The two EESAs are mounted on a ∼0.5 m boomlet alone while the two PESAs and SSTs are on an opposing ∼0.5 m boomlet. The top-hat hemispheres are lined with gold black coating to reduce scattered light/glint within the detector. A grid at the analyzer exit prevents leakage fields from the MCP from entering the analyzer section (i.e., top-hat part). Both EESA High and PESA High have 24 discrete anodes while EESA Low and PESA Low only carry 16. The orientation of the detectors is such that the anodes define the poloidal (with respect to the spin axis of the spacecraft) angular resolution. They are arranged such that there are eight anodes with ∼5.625° resolution for the anodes within ±22.5° of the spin plane[8], four anodes (two on each side of the eight) with ∼11.25° resolution between ∼22.5° and ∼45° of the spin plane, and the remaining anodes all have ∼22.5° resolution. Although each ESA has at least 16 discrete anodes, they are often averaged onboard down to an eight anode equivalent. The charge pulses produced by the electron showers emitted from the MCPs hit an anode and are sent to a pre-amplifier-discriminator (specifically a AMPTEK A111) and then accumulated into a 24-bit counter (specifically a 8C24) mounted on the amplifier board. The MCPs are mounted in a chevron pair configuration and designed to produce a gain of $\sim 2\times10^6$ with a narrow pulse height distribution. Each of the two MCPs are ∼1 mm thick with a bias angle of ∼8°. The analyzers are swept logarithmically in energy and the counters are sampled 1024 times per spacecraft spin (∼3 ms sample period) Below we discuss each detector individually.

The SSTs consist of either a pair or triplet of closely-sandwiched silicon detectors. One SST end is covered by a thin lexan foil (SST Foil), to stop protons up to ∼400 keV, with 1500 Å of aluminum evaporated on each side to eliminate sunlight. The oposite end is not covered but open (SST Open) and is lined by a common broom magnet to sweep away electrons below ∼400 keV. The center detector of the triplet has an area of ∼1.5 cm^2 and is ∼0.5 mm thick (SST Thick), while all other silicon wafers are ∼1.5 cm^2 by ∼0.3 mm thick. Each double-ended telescope has two $36^\circ\times20^\circ$ fields-of-view (FOVs) at FWHM, thus each detector type acts like six telescopes (i.e., one SST Foil telescope has two sets of silicon wafer detectors). Therefore, five of the telescopes for each type can cover a $180^\circ\times20^\circ$ slice of the sky. The rotation of the spacecraft gives a complete 4π steradian coverage. Both ends of telescope 2 are covered with a drilled tantalum cover that acts as an attenuator for the most intense particle events (i.e., reduces the geometric factor by 10). The collimators on the SST Open sides prevent sunlight from directly hitting the silicon wafers on all six Open telescopes except 5. The inside of the collimators are blackened to reduce scattered light. The electronics were designed to recover quickly (within ∼130 ms) from the current pulse generated during exposure to the Sun, i.e., only 30° of rotation are lost for Open telescope 5. The ion-implanted silicon wafers were designed to have exceptionally low leakage currents of $\lesssim$10 nA at

[7]High and low also refer to the sensitivity of the instrument as the fluxes at low energies vastly exceed those at higher energy ranges.

[8]Note that the spin plane of *Wind* is always aligned to within $\lesssim1^\circ$ of the ecliptic plane.

room temperature.

- **EESA Low (EL):** Measures electrons from ∼3 eV to ∼1 keV though after 2000 most times span ∼5 eV to ∼1.1 keV. The detector has a 180° × 14° FOV and 16 discrete anodes, i.e., the angular acceptance angle is ±7° (7.5° FWHM). The top-hat has an inner hemispherical radius of ∼3.75 cm (R) with a separation of ∼0.28 cm (ΔR) and a top-cap separation of ∼0.56 cm. This gives an entrance opening half angle of ∼19°. The energy resolution is $\Delta E/E$ ∼ 20% FWHM. The electrons exiting the top-hat ESA are post-accelerated by at least a +500 V potential (commandable and changed over mission lifetime as MCPs slowly degrade) to increase the detection efficiency to ∼70%. A single attenuator grid results in a total geometric factor of 1.26×10^{-2} E cm^2-sr (where E is energy in eV). All particle distribution returned by this instrument using the software[9] written by *Wilson III* [2021] have 15 energy bins and 88 solid angle bins, whether in burst or survey mode. The total integration time for this instrument is always one spin period (∼3 s) but the time betwen distributions (i.e., between the center time of each) can vary between spin resolution in burst mode to ∼24–78 s in survey mode. EL does not have an anti-coincidence detector. The nominal dynamic range is ∼10^2–10^9 eV cm^{-2} sr^{-1} s^{-1} eV^{-1}.
- **EESA High (EH):** Nominally measures electrons from ∼100 eV to ∼30 keV but most distributions have energies varying from a minimum of ∼137 eV to a maximum of ∼28 keV. The detector has a 360° × 90° FOV and 24 discrete anodes, i.e., the angular acceptance angle is ±45°. Although EH has the same $\Delta R/R$ and opening angle as EL, electrostatic deflectors increase the FOV from ±7° to ±45°. Leakage fields from these deflectors are minimized by a pair of grids at the outer analyzer collimator. The top-hat has an inner hemispherical radius of ∼8.0 cm with a separation of ∼0.6 cm and a top-cap separation of ∼1.2 cm. This gives an entrance opening half angle of ∼19° like that of EL. The energy resolution is $\Delta E/E$ ∼ 20% FWHM. The MCPs are surrounded by an L-shaped plastic anti-coincidence scintillator, thus allowing the detector to reject MCP pulses coincident with light pulses. The optical geometric factor of the analyzer is ∼0.20 E cm^2-sr. Combining this with an MCP efficiency of ∼70% and a grid transmission (3 separate grids) of ∼73% results in a total geometric factor of ∼0.1 E cm^2-sr. All particle distribution returned by this instrument using the software written by *Wilson III* [2021] have 15 energy bins and 88 solid angle bins, whether in burst or survey mode. The total integration time for this instrument depends upon whether its in survey or burst mode, varying between ∼3 s in burst mode to several minutes in survey mode. Unlike EL, the time between EH center times is often the same as the total integration times. The nominal dynamic range is ∼10^0–10^8 eV cm^{-2} sr^{-1} s^{-1} eV^{-1}.
- **PESA Low (PL):** Nominally measures ions from ∼3 eV to ∼30 keV but most times span either ∼100 eV to ∼10 keV or ∼700 eV to ∼6 keV. PL is nearly identical to EL and only differences will be listed here. After existing the top-hat analyzer, ions are post-accelerated by an electrostatic grid located ∼1 mm above the MCP by voltages ≤ -2500 V (commandable and changed over mission lifetime as MCPs slowly degrade) to improve detection efficiency. Due to the intensity of the cold, fast solar wind beam, the PL detector has a collimator/attenuator to reduce the instrument response by a factor of 50. This collimator/attenuator has ∼0.24 mm diameter holes uniformly spaced in a ∼1 mm × ∼2.25 mm grid pattern. This results in a total geometric factor of 1.62×10^{-4} E cm^2-sr but an identical energy-angle response to that of PH. The total integration time for this instrument depends upon whether its in survey or burst mode, varying between ∼3 s in burst mode to several minutes in survey mode. All particle distribution returned by this

[9] reorganized and commented/documented versions of the original 3DP software libraries

instrument using the software written by *Wilson III* [2021] have 14 energy bins and 25(64) solid angle bins in survey(burst) mode. The nominal dynamic range is $\sim 10^4$–10^{11} eV cm^{-2} sr^{-1} s^{-1} eV^{-1}.

- **PESA High (PH):** Nominally measures ions from ∼3 eV to ∼30 keV but typically covers ∼500 eV to ∼28 keV. PH has the same physical top-hat schematics as PL except that PH has a 360° FOV and 24 anodes instead of 16. PH also has a post-acceleration grid above (before) the MCP to increase ion detection efficiency. Similar to EH, PH has an anti-coincidence scintillator surrounding the MCPs for rejecting light pulses. The optical geometric factor of the analyzer is 0.04 E cm^2-sr, combined with a MCP efficiency of 50% and a grid entrance post-transmission of 75%, while the total geometric factor is ∼0.015 E cm^2-sr. The total integration time for this instrument depends upon whether its in survey or burst mode, varying between ∼3 s in burst mode to several minutes in survey mode. All particle distribution returned by this instrument using the software written by *Wilson III* [2021] have 15 energy bins and five possible solid angle bin settings[10], commandable from ground, for both survey and burst mode. The nominal dynamic range is $\sim 10^1$–10^9 eV cm^{-2} sr^{-1} s^{-1} eV^{-1}.
- **SST Foil (SF):** Nominally measures electrons from ∼25–400 keV but often spans ∼27–520 keV. Each of the telescopes has a geometric factor of ∼0.33 cm^2-sr for a combined value of ∼1.65 cm^2-sr for the five telescope set. The total integration time for this instrument depends upon whether its in survey or burst mode, varying between ∼3 s in burst mode to ∼12 s in survey mode. All particle distribution returned by this instrument using the software written by *Wilson III* [2021] have 7 energy bins and 48 solid angle bins in both survey and burst mode. The nominal dynamic range is $\sim 10^{-1}$–10^6 eV cm^{-2} sr^{-1} s^{-1} eV^{-1}.
- **SST Open (SO):** Nominally measures protons from ∼20–6000 keV but often spans ∼70–6700 keV. Like SF, each of the telescopes has a geometric factor of ∼0.33 cm^2-sr for a combined value of ∼1.65 cm^2-sr for the five telescope set. The total integration time for this instrument depends upon whether its in survey or burst mode, varying between ∼3 s in burst mode to ∼12 s in survey mode. All particle distribution returned by this instrument using the software written by *Wilson III* [2021] have 9 energy bins and 48 solid angle bins in both survey and burst mode. The nominal dynamic range is $\sim 10^{-1}$–10^6 eV cm^{-2} sr^{-1} s^{-1} eV^{-1}.
- **SST Foil+Thick (FT):** Nominally measures electrons from ∼400 keV to >1 MeV. There are two telescopes giving a $72° \times 20°$ FOV and total geometric factor of ∼0.36 cm^2-sr (one, telescope 6, has a geometric factor of ∼0.33 cm^2-sr the other, telescope 2, ∼0.03 cm^2-sr). The total integration time for this instrument depends upon whether its in survey or burst mode, varying between ∼3 s in burst mode to ∼12 s in survey mode. All particle distribution returned by this instrument using the software written by *Wilson III* [2021] have 7 energy bins and 16 solid angle bins in both survey and burst mode. The nominal dynamic range is $\sim 10^{-2}$–10^6 eV cm^{-2} sr^{-1} s^{-1} eV^{-1}.
- **SST Open+Thick (OT):** Nominally measures protons from ∼6–11 MeV. OT has the same FOV and geometric factor as FT as they are on opposite ends of the same telescope pair. The total integration time for this instrument depends upon whether its in survey or burst mode, varying between ∼3 s in burst mode to ∼12 s in survey mode. All particle distribution returned by this instrument using the software written by *Wilson III* [2021] have 9 energy bins and 16 solid angle bins in both survey and burst mode. The nominal dynamic range is $\sim 10^{-2}$–10^6 eV cm^{-2} sr^{-1} s^{-1} eV^{-1}.

[10] i.e., distributions can have one of the following number of solid angle bins: 121, 97, 56, 65, or 88

2.3 WAVES Instrument

Physical Specs: The *Wind* WAVES instrument is comprised of three orthogonal electric field antenna and three orthogonal search coil magnetometers. The electric field antenna are dipole antennas with two orthogonal wire antennas in the spin plane and one spin axis stacer antenna. The spin plane wire antennas have a diameter of ∼0.38 mm; are made of seven strands of BeCu with a mass density of ∼1.1 g/m; and are capped by a tip mass of ∼10.5 g. The spin axis stacer antennas have a diameter of ∼28.4 mm; are made of polished silver-plated BeCu with a mass density of ∼85.0 g/m; and are capped by a tip mass of ∼52.2 g. The spin plane antennas have mechanical, tip-to-tip lengths of 100 m (x-antenna) and 15 m (y-antenna). The spin axis stacer antennas have a mechanical, tip-to-tip length of 12 m (z-antenna) [*Bougeret et al.*, 1995; *Wilson III*, 2010; *Wilson III et al.*, 2010].

All conducting materials in a plasma will exhibit a sheath region due to the combination of plasma thermal currents and photoelectron currents due to incident ionizing radiation, resulting in non-zero spacecraft floating electric potential fields. These sheaths reduce the mechanical length of electric field antennas to what is called an *effective antenna length* that is usually shorter than the mechanical length. The initial effective antenna lengths are ∼41.1 m, ∼3.79 m, and ∼2.17 m for the x-, y-, and z-antenna, respectively. The electric field antennas on *Wind* operate as dipoles, thus one of the monopoles is assigned a positive and the other a negative value. The +x-antenna has broken twice since launch, once on August 3, 2000 around ∼21:00 UTC and September 24, 2002 around ∼23:00 UTC[11]. These breaks reduced the effective antenna length the x-antenna from ∼41.1 m to ∼27 m after the first break and ∼25 m after the second break [e.g., see discussion in *Malaspina and Wilson III*, 2016; *Malaspina et al.*, 2014].

The search coils contain a 4 mil supermalloy laminated bar with a radius and length of ∼4.7625 mm and ∼393.7 mm, respectively. The initial permeability was $\mu_i \sim 60{,}000$ at 100 Hz. The effective permeability of the rod was found to be $\mu_e \sim 1738$. The search coils contain 5715 turns of #44 AWG wire per section for a total of 40,005 turns per bobbin. There is an additional 1000 turns of #40 AWG wire in the eighth section of the bobbin for calibration [see *Hospodarsky*, 1992, for detailed discussion and calibration].

Measurements: The *Wind* WAVES instrument measures electric and magnetic fields in two ways: as a remote radio receiver for spectrograms and as an in situ instrument for time series vector fields. The WAVES radio receiver is comprised of four receivers: Low Frequency FFT receiver or FFT (∼few to ∼11 kHz), Thermal Noise Receiver or TNR (∼4–256 kHz), radio receiver band 1 or RAD1 (∼20–1040 kHz), and radio receiver band 2 or RAD2 (∼1.075–13.825 MHz). Unfortunately, the FFT receiver, which covers ∼few to ∼10 kHz is dominated by noise and therefore rarely used and not publicly available. The TNR, RAD1, and RAD2 receivers, however, are extremely well calibrated and highly utilized. The radio data are measured either with as a multi-channel, band-limited Fourier spectrum (TNR) or swept frequency response (RAD1 and RAD2). For details about the TNR bands, see Table 6.

The WAVES instrument contains two more receivers that record high cadence electric and magnetic fields in time series form. These are the time domain sampler (TDS) receivers. There are two of them, one fast (TDSF) and one slow (TDSS). The TDSF data are always comprised of two electric field components called channels. Channel 1 is always the x-antenna and Channel 2 can be commanded to be the y- or z-antenna. Nearly all TDSF waveform captures use the x- and y-antennas. The TDSS receiver returns four vector fields of three magnetic(electric) and one electric(magnetic) field components. Any combination of channels can be commanded to the

[11]The exact times of the break are not known due to the data products necessary to determine a break not having 100% coverage. These are the current best guesses.

Table 6: Wind WAVES TNR Specs

Band	Range (kHz)	Sampling Rate (kHz)	Measurement Time (ms)
A	4-16	64.1	320
B	8-32	126.5	160
C	16-64	255.7	80
D	32-128	528.5	40
E	64-256	1000.0	20

spacecraft provided there is three magnetic(electric) and one electric(magnetic) field components. Both TDSS and TDSF have commandable sample rates from ∼117 sps to 7500 sps for TDSS and from ∼1800 sps to 120,000 sps (see Table 7 for specific modes). All TDS waveform captures, called TDS events for brevity, have 2048 time steps per field component. When in its highest sampling rate, the TDSF data have little to no gain below ∼120 Hz so the data are high pass filtered at ∼150 Hz in the data documented by *Wilson III* [2023]. The search coils show a gain roll off ∼3.3 Hz, thus are not DC-coupled [e.g., see *Wilson III*, 2010; *Wilson III et al.*, 2010, 2012, 2013, and references therein for more details]. The instrument related sections of this paper are reproduced at the *Wind* project webpage[12]. Some additional documentation exists also at the WAVES instrument webpage[13]. The content and format of the various WAVES data products are also described on the instrument webpage.

Table 7: Wind WAVES TDS Specs

Speed	Fast Sampler (sps)	Slow Sampler (sps)
A	120,000	
B	30,000	
C	7,500	7,500
D	1,875	1,875
E		468
F		117

[12] https://wind.nasa.gov
[13] https://spdf.gsfc.nasa.gov/pub/data/stereo/documents/websites/solar-radio/wind/index.html

2.4 SWE Instrument

The *Wind* SWE instrument consists of three separate detectors: two Faraday cup (FC) sensors; a vector electron and ion spectrometer (VEIS); and a strahl[14] sensor (Strahl). Nominally, both the FCs and the VEIS detectors can measure ions while the Strahl detector only electrons. However, the high voltage power supply failed on VEIS on May 31, 2001 reducing the SWE capabilities to the FCs for ions and Strahl detector for electrons. The discussion below will be taken from *Ogilvie et al.* [1995], *Kasper* [2002], and *Kasper et al.* [2006]. The detectors' specifications and nominal ranges are shown in Table 8.

Table 8: SWE Detector Specs [altered from Table II in *Ogilvie et al.* [1995]]

Comments	**FCs**	**VEIS**	**Strahl**
Energy/charge Range[a] [keV/e]	∼0.15–8.0	∼0.007–24.8	∼0.005–5.0
Resolution at FWHM			
$\Delta(E/Q)/(E/Q)$	∼6.5–13%	∼6%	∼3%
Total Instrument Geometry Factor			
GF [cm^2 sr]	∼110	∼0.00046	∼0.0007
FOV[b]	N/A	7.5° × 6.5°	≈ 3° × ±30°

[a] nominal and/or design values/measurements; [b] field-of-view;

VEIS: The *Wind* VEIS detector is comprised of two units each with three separate ESAs, i.e., six ESAs total. The instrument was nominally intended to measure ions and electrons over an energy-per-charge range of ∼0.005–24.8 keV/e with 16 logarithmically spaced energy bins and a resolution of $\Delta(E/Q)/(E/Q) \sim 6\%$. Ions and electrons were measured sequentially by flipping the sign of the electric potential in the ESAs. The particles were detected using channel electron multipliers. The FOV for each ESA, 7.5° × 6.5°, is determined entirely by a collimator at the entrance to the ESA and the sensitive area of the detector. Thus, each analyzer has geometric factor of ∼0.00046 cm^2-sr for a total geometric factor of ∼0.00276 cm^2-sr. The hemispherical plates have radii of ∼4.717 cm and ∼5.443 cm. Near the entrance, the outer hemispherical plate of the ESA has a mesh-covered hole to serve as a light trap. Between the exit of the ESA and the channeltron there is a high-transparency mesh grid to prevent electric field leakage between the two sections. These features help improve the accuracy of the solid angle knowledge and greatly reduce the responses resulting from photoelectrons produced inside the detector. Note, there two channeltrons per analyzer, one for electrons and one for ions. The gains of each of the six analyzers must be known to ∼1%. This was achieved using UV photons to excite each detector to provide a stable relative calibration for each.

FC: The *Wind* FCs are located on the top and bottom of the spacecraft bus, each pointed ∼15° away from the spin plane of the spacecraft, i.e., the FC normals are pointed ∼15° above and below the ecliptic plane. Each FC has nine grids, one acting as a square-wave modulator at 200 Hz, one biased to -130 V located just above the collecting plates and seven more grounded grids located on either side of the the modulator grid and the collecting plates (three above, four below). The modulator acts as to define the energy-per-charge of the incident ions and to discriminate between charged particles and the photoelectric currents generated by sunlight. The biased grid acts as the suppressor, i.e., to prevent the loss of secondary electrons from the collector plates. The outermost

[14] German for beam, the strahl is the magnetic field-aligned, anti-sunward (usually) electron population typically seen with E ∼ few 10s of eV.

grounded grids reduce the emission of time-varying electric fields near the front/aperture of the sensor. The gounded grids between the modulator and suppressor grids reduce the capacitively-coupled currents induced by the modulator electric fields. The collector plates are semi-circular in shape (i.e., hemispheres) and are connected to preamps to measure the net current incident on the plate. The currents are inverted to estimate a model reduced velocity distribution function for both protons and alpha-particles. Each of the FCs have a total collecting area of ∼34 cm^2 for normal incidence particles, a FOV of ∼ 121° × 121°, an energy-per-charge range of ∼0.15–8.0 keV/e over 64 logarithmically spaced energy bins and a resolution of $\Delta\left(E/Q\right)/\left(E/Q\right) \sim 6.5$–13%, and a total geometric factor of ∼110 cm^2-sr. When the detector is in a mode that uses a ∼30 ms integration time, the instrument can measure net currents in the range of $\sim 3 \times 10^{-7}$ to $\sim 3 \times 10^{-2}$ μA (i.e., $\sim 3 \times 10^{-7}$ μA is the thermal noise level for a ∼30 ms integration time).

Strahl: The *Wind* Strahl detector is a truncated, toroidal electrostatic analyzer that bends particles through ∼131° before they hit a MCP stack with anodes behind. The instrument's original design had a FOV of ∼ 3° × ±30°. There are two channel plates, with six anodes per plate, each covering ∼5° of the sky (i.e., ∼30° total per plate). The detector has an energy-per-charge range of ∼0.005–5.0 keV/e with a resolution of $\Delta\left(E/Q\right)/\left(E/Q\right) \sim 3\%$ using 16 logarithmically spaced energy bins. In its original configuration, the instrument would step the energy only once per spin, thus requiring 16 spins to complete the energy sweep. The detector has a geometric factor of ∼0.0007 cm^2-sr per anode, i.e., total of ∼0.0084 cm^2-sr. The two toroidal plates have inner radii of ∼5.40 cm and ∼14.4 cm while the outer radii are ∼6.60 cm and ∼15.6 cm.

After the failure of VEIS, Strahl was reconfigured to have 13 energy channels with eight azimuthal angle bins (each ∼45° wide) and six poloidal/elevation bins (each ∼9° apart) for a total of 624 measurements accumulated over three spacecraft rotations, i.e., ∼9 seconds in duration. The poloidal angles are defined by the anodes, the azimuthal by the spacecraft rotation, and the energy by the toroidal plate potentials. Assuming the spacecraft spin axis is directed exactly along the south ecliptic direction, then the mid-point look direction of the six poloidal angles relative to the ecliptic plane are: -26.55°, -17.10°, -7.34°, +7.63°, +17.10°, and +26.53°. The 13 energies were[15] as follows: 19.34 eV, 38.68 eV, 58.03 eV, 77.37 eV, 96.71 eV, 116.1 eV, 193.4 eV, 290.1 eV, 425.5 eV, 580.3 eV, 773.7 eV, 1006 eV, and 1238 eV. These values correspond to electron speeds ranging from ∼2608 km/s to ∼20,830 km/s. The result is three data products described in Section 4.2.

[15]The past tense is used here because these energy bin values may change over time (for various reasons related to detector aging) and the documentation is specific to when the instrument was originally reconfigured.

2.5 SMS Instrument

The *Wind* SMS instrument consists of three separate detectors: the Solar Wind Ion Composition Spectrometer (SWICS), the high-resolution MASS spectrometer (MASS), and the Supra-Thermal Ion Composition Spectrometer (STICS). The SWICS and STICS detectors can measure ions from hydrogen (H) to iron (Fe) and MASS from helium (He) to neon (Ne). The SWICS and STICS detectors can determine mass-per-charge (M/Q) from 1–30 and 1–60, respectively. As discussed in Section 1.2, the SWICS detector was turned off in May 2000 so it's no longer producing data. The MASS detector has suffered a few incidents of degradation in its acceleration power supply, thus the publicly available data from this detector are limited. The majority of the science quality data produced by SMS comes from STICS, which is still actively producing new data and new data products. The discussion below will be taken from *Gloeckler et al.* [1995], *Gruesbeck* [2013], and *Chotoo* [1998]. The detectors' specifications and nominal ranges are shown in Table 9.

SWICS: The *Wind* SWICS detector is a time-of-flight (TOF) mass spectrometer, capable of measuring the mass (M), mass-per-charge (M/Q), and energy (E) of incident particles. Ions enter the electrostatic deflection analyzer through a large-area, conical, multi-slit collimator then pass through a TOF system. The entire assembly gives STICS an energy-per-charge, mass-per-charge, and mass resolution of $\Delta\left(E/Q\right)/\left(E/Q\right) \sim 6\%$ FWHM, $\Delta\left(M/Q\right)/\left(M/Q\right) \sim 4\%$ FWHM, and $\Delta M/M \sim 20\%$ FWHM[16], respectively. The SWICS detector covers the energy-per-charge range of ∼0.5–30 keV/e with a total geometric factor of ∼0.0023 cm^2-sr and a FOV of $4° \times 45°$.

The width of the collimator channels are designed such that they limit dispersion and flight path differences in the TOF system to $< 0.5\%$. The deflection system is conical in shape, has a small angle, and is pie-shaped with ∼45° deflection plates. These deflection plates are connected to a variable power supply that cycles through 60 logarithmic energy steps, separated by ∼7%, one step per spacecraft spin (i.e., once every ∼3 seconds). The deflection system uses a combination of serration, black-coating, and light traps to eliminate stray or reflected light and UV radiation. This deflection system defines the energy-per-charge resolution and is used for the mass versus mass-per-charge analysis.

Ions are post-accelerated by up to ∼30 kV after exiting the deflection system, before entering the TOF system. The post-acceleration energy gain after the collimator is necessary for depositing enough energy in the solid state detector (SSD), which typically have a ∼25–35 kV threshold. After this, the ions strike a thin (∼2 μg cm^{-2}) carbon foil[17], supported on an ∼85% transmission nickel grid, at the entrance to the TOF telescope. The ion will pass through and eject at least one secondary electron that strikes the start MCP detector. Behind the MCP are two discrete anodes to help provide elevation angle information. The ion propagates ∼10.5 cm to a SSD[18], the gold front surface of which acts as the electron source for the second, stop MCP. The electrons are deflected toward the start and stop MCPs by a common ∼1 kV power supply, which negligibly affects the ions. The difference in flight path between the secondary electrons only introduces a ∼0.5 ns FWHM timing uncertainty. Thus, the instrument measures or sets or knows the TOF time, τ, incident energy-per-charge, E/Q, residual energy, E_{res}, post-acceleration voltage, ϕ_a, TOF path length, d, energy-per-charge accounting for small loss at start foil, E'/Q, and the nuclear defect [e.g., see *Ipavich et al.*, 1978] in the SSDs, α. From these one can calculate the the mass (M), mass-per-charge (M/Q), charge state (Q), incident energy (E), and incident speed (V_{inc}):

[16] $\Delta M/M$ is species-dependent

[17] *Gruesbeck* [2013] shows an example estimate of the energy loss due to the carbon foil for an oxygen atom, with an initial kinetic energy of ∼78.81 keV, to be ∼4.42 keV for the STICS TOF system.

[18] The SSD is gold-silicon (Au-Si) wafer.

$$M = 2\left(\frac{\tau}{d}\right)^2 \left(\frac{E_{res}}{\alpha}\right) \tag{1a}$$

$$Q = \frac{E_{res}/\alpha}{\phi_a + E'/Q} \tag{1b}$$

$$\frac{M}{Q} = 2\left(\frac{\tau}{d}\right)^2 \left(\phi_a + E'/Q\right) \tag{1c}$$

$$E = Q\left(\frac{E}{Q}\right) \tag{1d}$$

$$V_{inc} \approx 438\sqrt{\frac{E}{M}} \tag{1e}$$

where the units of V_{inc} are km/s for E/M in units of keV/amu.

Table 9: SMS Detector Specs [altered from Table I in *Gloeckler et al.* [1995]]

Comments	**SWICS**	**MASS**	**STICS**
Ion Species[a]	H–Fe	He–Ni	H–Fe
Mass/charge Range[a] [amu/e]	1–30	N/A	1–60
Energy/charge Range[a] [keV/e]	∼0.5–30	∼0.5–11.6[b]	∼8–226
Resolution at FWHM			
$\Delta(E/Q)/(E/Q)$	∼6%	∼5%	∼5%
$\Delta(M/Q)/(M/Q)$	∼4%	N/A	∼15%
$\Delta M/M$ ∼20%[b]	∼1%[b]	∼12%[c]	
Total Instrument Geometry Factor			
GF [cm^2 sr]	∼0.0023	N/A	∼0.05
gf [cm^2]	∼0.018	∼0.35	N/A
FOV[d]	4° × 45°	4° × 40°	4.5° × 156°
Other Paramters			
Dynamic Range[a]	10^{10}	10^{10}	5×10^{10}
Min eflux[e,a] [cm^{-2} sr^{-1} s^{-1} $(keV/e)^{-1}$]	N/A	10^{-6}	N/A
Min iflux[f,a] [cm^{-2} s^{-1}]	10^{-2}	10^{-2}	N/A

[a] nominal and/or design values/measurements; [b] species-dependent; [c] STICS only measures mass above ∼30–100 keV, depending on species; [d] field-of-view; [e] energy flux [f] integrated number flux

The total residual kinetic energy, E_{res}, is measured by one of three low-noise, rectangular SSDs. The center SSD is used for bulk/thermal solar wind ions when the instrument points at the sun (i.e., once per spin) and for suprathermal ions for all other pointing directions. The two side detectors primarily measure suprathermal ions for all pointing directions. Together, the three SSDs have a combined FOV of ∼45° for one pointing direction. By sectoring the respective outputs, one can determine anisotropy information above, below, and in the ecliptic plane.

MASS: The *Wind* MASS detector is a mass spectrometer capable of distinguishing the elemental and isotopic solar wind ion composition. Like SWICS, MASS employs an electrostatic deflection system and a TOF mass analyzer system. However, the electrostatic deflection system for MASS is spherical in shape and operates as a UV trap and energy-per-charge discriminator/filter. The

entire assembly gives MASS an energy-per-charge and mass resolution[19] of $\Delta\,(E/Q)\,/\,(E/Q) \sim 5\%$ FWHM and $\Delta M/M \sim 1\%$ FWHM, respectively. The MASS detector has an energy-per-charge range[20] of ∼0.5–11.6 keV/e total integrated (over solid angle) geometric factor is ∼0.35 cm^2.

The ions enter the spherical hemispheres of the electrostatic deflection system, which has a mean radius of ∼107.75 mm with a separation of ∼4.50 mm, deflecting the original particle trajectory by ∼128°. The hemispheres have a voltage range from ∼ -0.077 kV to ∼ +1800 kV in 64 logarithmic energy steps. After passing through the the electrostatic deflection system the ions impact a thin carbon foil.

The ions retained their charge state through the electrostatic deflection system. At the start of the TOF system is a 4 x 15 mm, grid-supported, ∼2 μg cm^{-2} thin carbon foil. Unlike the ions passing through the foil in SWICS, these ions mostly reach a neutral or singly charged state, with a smaller fraction of incident ions retaining final charge states, Q^*, satisfying $Q^* \geq +2$ or $Q^* \leq$ -1. As the ion emerges from the foil, a few to a few tens of secondary electrons are ejected. These electrons are accelerated to a start MCP that begins the TOF system timing. Only those ions that have $Q^* \geq +1$ are accelerated in the opposite direction to their original incidence toward a large area (∼10.0 x 1.5 cm) stop MCP (i.e., ion path through electrostatic deflection system to the stop MCP has an S-shape).

The electric potential used to accelerate the particles in the TOF system is not a static, constant potential, but depends upon spatial position, z, normal to the carbon foil and stop MCP surface. That is, the ions enter the TOF system through the carbon foil at $z = 0$ (with a non-normal angle of incidence) and are deflected through an arc (with $z > 0$) returning to the stop MCP also at $z = 0$. The magnitude of the electric potential satisfies $\phi \propto z^2$. This profile is achieved by putting the TOF system between a positively charged, hyperbolically-shaped potential plate and a V-shaped, low potential plate. In such a potential, the TOF duration, τ, depends only upon the mass-per-charge, i.e., $\tau \propto \left(\frac{M}{Q^*}\right)^{1/2}$. Since τ is accurately measured to fractions of a nanosecond and the magnitudes of τ tend to satisfy ∼60–460 ns, the ion mass can be measured to a high degree of accuracy for Q^* = +1 ions.

The entire TOF system floats at an adjustable potential, $\phi_{A/D}$, relative to the electrostatic deflection system. This floating potential has 256 linearly-spaced values between ∼ -6.0 kV and ∼ +1.7 kV. The value of $\phi_{A/D}$ is adjusted once per spin, where negative values accelerate lower energy ions to increase the fraction of $Q^* = +1$ ions exiting the foil and postive values are used to decelerate higher energy ions to contain them within the TOF system (i.e., so they don't hit the surface opposite the stop MCP).

STICS: The *Wind* STICS detector is a TOF mass spectrometer, capable of measuring the mass (M), charge state (Z), and energy (E) of incident particles. The detector is composed of three telescopes, oriented to view latitude sectors[21] and rely on the spacecraft spin to map out nearly the full 4π steradian sky. Ions enter through an aperture opening and immediately pass through an ESA similar to the concept behind the 3DP top-hats but STICS has an angular acceptance angle of ∼4.8°. The ESA serves as a UV trap and an energy-per-charge discriminator/filter. The azimuthal sectors are divided into 16 equally sized bins, each spanning ∼22.5°. The STICS detector covers the energy-per-charge range of ∼6.2–223.1 keV/e with a total geometric factor of ∼0.05 cm^2-sr and a FOV of 4° × 156°.

[19] both energy and mass resolution are species-dependent

[20] energy range is also species-dependent

[21] The sector angles, relative the spacecraft spin plane (i.e., 0° is in spacecraft spin plane), are as follows: Telescope 1 covers +79.5° – +26.5°, Telescope 2 covers +26.5° – −26.5°, and Telescope 3 covers −26.5° – −79.5°.

The spherical hemispheres have a mean radius of ∼107.75 mm with a separation of ∼4.50 mm with a voltage range from ∼0.263 kV to ∼9.45 kV, deflecting the original particle trajectory by ∼125°. The hemisphere voltage difference is stepped through 30 times on a logarithmic scale allowing the detector to discriminate the particle's energy-per-charge over the range ∼6.2–223.1 keV/e for a resolution of $\Delta\left(E/Q\right)/\left(E/Q\right) \sim 5\%$ FWHM. The voltage is stepped once every two spins, which corresponds to ∼180 seconds for a full energy sweep. The STICS TOF assembly is very similar to that of SWICS described above except there is no post-acceleration grid after the ESA and the TOF path length is ∼10 cm instead of ∼10.5 cm. The lack of post-acceleration also implies the lower energy ions will not register in the SSD. Once the ions hit the SSD, two events will occur: (1) if the incident ion's total energy exceeds the threshold energy of the SSD, i.e., ∼30–35 keV, then the ion's energy can be measured; (2) the incident ion ejects another secondary electron from the SSD which is measured by a second MCP to determine the stop signal. The duration between start and stop times allows the instrument to calculate the particle speed since the telescope length is well defined at 10 cm. The entire assembly gives STICS a mass-per-charge and mass[22] resolution of $\Delta\left(M/Q\right)/\left(M/Q\right) \sim 15\%$ FWHM and $\Delta M/M \sim 12\%$ FWHM, respectively. Additional details of the instrument calibration, operation, and data products can be found in *Gruesbeck* [2013] and *Chotoo* [1998].

The properties of each observed particle (i.e., mass, mass-per-charge, and energy) are calculated onboard. This data is saved and sent to ground. The instrument also creates pulse height analyzed (PHA) words for a subset of the observed particles. Each PHA word contains the measured TOF, energy, and observation direction information. From this, the element, charge state, and velocity of the particle can be determined. Using the combination of this information, one can construct the phase space density distribution for each ionic species. The data products currently available (as of August 15, 2024) are H^{+} and He^{2+}, both separated into observations made in the magnetosphere and those in the solar wind (e.g., see Section 4.4). Eventually, the following additional ion species data are to be released: He^{+}, C^{+}, C^{2+}, C^{5+}, O^{+}, O^{6+}, and Fe^{10+}.

[22] Only measures mass for ions with $E \gtrsim$ 30–100 keV, depending on species.

2.6 EPACT Instrument

The *Wind* EPACT instrument consists of three separate detectors: the Low Energy Matrix Telescope (LEMT); the Electron Isotope Telescope (ELITE); and the Suprathermal Energetic Particle (STEP) telescope. The ELITE system contains three separate telescopes comprising two Alpha-Proton-Electron (APE) telescopes (APE-A and APE-B) and one Isotope Telescope (IT). The LEMT system is also composed of three telescopes, but all measure the same particles. The STEP system contains two identical telescopes. All telescopes except STEP use the "dE/dx vs E" method to identify particles relying on solid state detectors (SSDs). The STEP telescopes measure time-of-flight (TOF) and energy using start and stop MCPs in combination with a SSD to measure the total energy (similar to the SMS STICS design discussed in Section 2.5). As discussed in Section 1.2, the ELITE system had a major failure in its HVPS in 1995 resulting in only APE-B returning one energy channel of protons between ∼5 and ∼20 MeV while IT and APE-A return nothing. The discussion below will be taken from *von Rosenvinge et al.* [1995b], *Chotoo* [1998], *Filwett et al.* [2017], and *Filwett et al.* [2019]. The detectors' specifications and nominal ranges are shown in Table 10.

Table 10: EPACT Detector Specs [altered from Table I in *von Rosenvinge et al.* [1995b]]

Comments	**LEMT**	**APE-A**	**APE-B**	**IT**	**STEP**
Ion Species[a]	H–U	e, H–Fe	e, H–Fe	He–Fe	He–Fe
Charge Range[a] [e]	+2 to 90	-1 to +26	-1 to +26	+2 to 26	+2 to 26
Energy Ranges					
Electrons [MeV][a]	N/A	∼0.2–2.0	∼1–10	N/A	N/A
Hydrogen [MeV][a]	∼1.4–10	∼4.6–25	∼19–120	N/A	∼0.1–2.5[b]
Helium [MeV/nucleon][a]	∼1.4–10	∼4.6–25	∼19–500	∼3.4–55	∼0.04–8.1
Iron [MeV/nucleon][a]	∼2.5–50	∼15–98	∼73–300	∼12–230	∼0.020–1.2
Total Instrument Geometry Factor					
GF [cm^2 sr]	∼3×17	∼1.2	∼1.3	∼9.0	∼2×0.4

[a] nominal and/or design values/measurements; [b] extra data product

STEP: The *Wind* STEP detector is a time-of-flight (TOF) mass spectrometer, capable of measuring the energy (E) and TOF duration of incident particles, which allows for the determination of mass (M). Ions enter a collimated sun shade and are incident on two thin (each ∼1000 Å thick) nickel foils. After emerging from the foils, ∼4–30 secondary electrons are ejected and are then deflected toward a start MCP by a ∼1 kV potential. The TOF system is ∼10.5 cm in length and it typically takes ions ∼2–100 ns to reach the SSD at the end of the TOF assembly. The nominal FOV is 17° × 44° (poloidal by azimuthal angles) with a total geometric factor of ∼0.4 cm^2-sr per telescope (two telescopes total). The two telescopes are pointed at ∼64° and ∼111° relative to the spacecraft spin axis[23]. The azimuthal scans of each telescope are divided into eight equal segments of ∼45°. STEP cannot distinguish the charge state of the ions but nominally measures charge states from ∼2–26 (though with careful effort hydrogen can be separated, as discussed below). The detector's energy range depends upon the species but can go well below 100 keV/nucleon for iron to over 8 MeV/nucleon for helium. The instrument is sensitive enough to distinguish the following ion populations: H^+, He^{2+}, CNO^{X+}, NeS^{X+}, and Fe^{X+}. That is, STEP can determine if an incident ion is in the carbon-nitrogen-oxygen group but cannot distinguish which of the three or its charge state. This diversity of ion groups is only available for longer integration times (i.e., ∼1 hr)

[23] The spin axis is pointed toward the south ecliptic pole

while the shorter integration times (i.e., ∼10 minutes) only allow for H^+, He^{2+}, CNO^{X+}, and Fe^{X+}.

LEMT: The *Wind* LEMT detector consists of three telescopes, each with 16 apertures covered by surface barrier detectors, SSDs, arrayed on a spherical dome. Each of these are ∼18 ± 0.34 μm thick and have surface areas of ∼1.75 cm^2. These top/outer detectors measure the dE/dx of the particle, i.e., its loss of energy with respect to spatial displacement through a solid material, the so called Bethe-Bloch effect[24] [e.g., see Chapter 13 of *Jackson*, 1998, for basic theory]. Each of the 16 surface SSDs have ∼0.3 mil (∼7.62 mm) kapton aluminum foil on inside surface and indium-tin-oxide foil (same thickness) on outside surface. Inside each of the three spherical domes, there is a residual energy, E, detector located directly behind (i.e., just under ∼6 cm from furthest dome inner surface) the spherical domes. This detectors, ion-implanted silicon (Si), are ∼1000 μm thick and have surface areas of ∼36 cm^2. They are subdivided into five ∼13.3 mm wide strips on each side (top and bottom), where strips are orthogonal on opposite sides. Each strip has its own, independent preamplifier. Behind the residual energy detector lies a ∼65 cm^2 x ∼1000 μm thick, ion-implanted Si, anti-coincidence detector. Each spherical dome has a total geometric factor of ∼17 cm^2-sr for a total of ∼51 cm^2-sr for the entire LEMT system. The instrument can nominally measure ions with charge states from ∼2–90 and particle energies from ∼1.4–50 MeV/nucleon. In practical use, the instrument usually measures helium to lead over ∼2–20 MeV/nucleon *Reames* [2017]. Each spherical dome has a nominal FOV of 126° × 126° and the spin of the spacecraft allows for full 4π sr coverage. LEMT does not determine charge state but it does determine the element. The publicly available data (e.g., see Section 4.5) includes hourly averaged omnidirectional spectra of He^{2+}, C^{X+}, O^{X+}, Ne^{X+}, Si^{X+}, and Fe^{X+}.

APE: The *Wind* APE detector consists of two telescope systems, APE-A and APE-B. APE-A is a single-ended telescope with a nominal FOV of 50° × 50°. The opening is covered by two thin foils to protect the detector from high count rates of lower energy particles and sunlight. The outer foil is ∼25 μm thick sheet of kapton. The inner foil is ∼12 μm thick sheet of aluminum. Below these foils are two silicon detectors, A1 and A2, and two lithium-drifted silicon detectors (LiDs), A3 and A4. The A1 and A2 detectors are silicon surface barriers that are each ∼8 cm^2 x ∼150 μm thick. The A3 and A4 detectors are circular LiDs that are each ∼17 cm^2 x ∼3000 μm thick. The geometry is defined by there being a coincidence between the A1 and A2 detectors combined with an anti-coincidence with the A4 detector. Much like LEMT, the detector uses the "dE/dx vs E" method to identify particles and cannot deduce the charge state. The total geometric factor of ∼1.2 cm^2-sr and the instrument nominally measures electrons and ions from hydrogen to iron, i.e., charge states satisfying -1 ≤ Q ≤ +26. Nominally, APE-A could measure electrons from ∼0.2–2.0 MeV, protons from ∼4.6–25 MeV, helium from ∼4.6–25 MeV/nucleon, and iron from ∼15–98 MeV/nucleon.

APE-B is a double-ended telescope with a nominal FOV of 54° × 42°. The larger (FOV-wise) opening is covered by two thin foils both made of ∼127 μm thick kapton. All of the LiDs in APE-B are silicon-based. Below these are two LiDs, B1 and B2, and each are ∼8 cm^2 x ∼2000 μm thick. Note that B1 is less than 1 cm from the foils but B2 is ∼6-7 cm below B1. Further, B1 and B2 are curved (mean radius of curvature ∼7.0 cm) to minimize pathlength variations of penetrating particles. Immediately below B2 are seven more LiDs. The first two, C1 and C2, are ∼17 cm^2 x ∼3000 μm thick. The remaining five, C3–C7, are ∼36 cm^2 x ∼3000 μm thick. Immediately following C7 is another LiD labeled D and is ∼17 cm^2 x ∼3000 μm thick. Below D are two more foils, from top(inner) to bottom(outer): ∼1020 μm thick aluminum foil and a ∼127 μm thick kapton

[24]The full corrections for real materials can be found in *Skyrme* [1967] and *Paul* [1971].

foil. Nominally, APE-B could measure electrons from ∼1–10 MeV, protons from ∼19–120 MeV, helium from ∼19–500 MeV/nucleon, and iron from ∼73–300 MeV/nucleon.

Particles entering on the B1-side are referred to as forwards particles and those on the D-side as backwards particles. Particles that pass through B1 and B2 but stop before C7 are called stopping particles and the total geometric factor for these particles is ∼1.3 cm^2-sr. Particles stopping in B2 are referred to as 2-D and those making it to C1–C6 are referred to as 3-D. Particles that pass through B1 and B2 and D are called penetrating particles. The total geometric factor[25] for penetrating particles is ∼1.95 x 1.08 cm^2-sr.

IT: The *Wind* IT detector consists of a single-ended telescope with a nominal FOV of $77° \times 77°$ with a total geometric factor of ∼9.0 cm^2-sr and charge states satisfying $+2 \leq Q \leq +26$. Similar to LEMT and the APE telescopes, IT uses the "dE/dx vs E" method to identify particles. The opening is covered by two thin foils to protect the detector from high count rates of lower energy particles and sunlight. The outer foil is a ∼19 μm thick sheet of kapton. The inner foil is ∼12 μm thick sheet of aluminum. Below these foils is a tungsten ring ∼380 μm thick with an inner radius of ∼5.61 cm. There are two tungsten rings, both immediately above a two-dimensional position sensitive detector (PSD), PSD1 and PSD2. The tungsten rings are vertically[26] separated by ∼7.02 cm. They sit ∼0.44 cm above each PSD. The PSDs are each ∼36 cm^2 x ∼150 μm thick of ion-implanted silicon. Each PSD is segmented into 125 strips with a pitch of ∼0.5 mm and an inter-strip gap of ∼35 μm. Preamplifiers are connected to strips 1, 32, 63, 94, and 125 to create four sections of 32 strips each on each PSD. If a particle is incident on a strip between 32 and 63, then the two preamps connected to those two strips will both measure pulse heights but the charge will be distributed between the two preamps proportional to the number of strips between impact location and the preamp strips (i.e., the closer preamp will measure more charge). Below the PSD2, there are three surface barrier (silicon) detectors, E1, E2, and E3. The separation between PSD2 and E1 and between E1 and E2 and E2 and E3 is ∼0.51 cm. These detectors have the following dimensions in order of E1, E2, and E3: ∼26 cm^2 x ∼110 μm thick, ∼34 cm^2 x ∼400 μm thick, and ∼70.3 cm^2 x ∼1000 μm thick. Below E3 by ∼0.35 cm is the first of four LiD detectors, E4, E5a, E5b, and E6[27]. The first three LiDs have dimensions of ∼57.3 cm^2 x ∼4000 μm thick. The last LiD, E6, has dimensions of ∼66 cm^2 x ∼3000 μm thick. There are a total of 26 preamplifiers attached to the stack of detectors, 10 for each of the two PSDs and one for each of surface barrier detectors (E1–E3) and one for each of the LiDs (E4–E6). Nominally, IT could measure helium from ∼3.4–55 MeV/nucleon and iron from ∼12–230 MeV/nucleon and the mass resolution was sufficient to easily distinguish the isotopes of helium and even those of magnesium.

[25] This accounts for the ∼5% view obstruction by the spacecraft bus on the backwards side of the telescope but ignores the possible obstruction due to the magnetometer boom in its FOV due to the small mass per unit area compared to the telescope detectors.

[26] Up is oriented here in such a way as to look along the telescope opening view direction, i.e., along the telescope axis.

[27] E6 acts as an anti-coincidence detector

2.7 KONUS Instrument

The *Wind* KONUS instrument consists of two identical sodium iodide (NaI) crystals activated with thallium (Tl), i.e., NaI(Tl) crystals [*Aptekar et al.*, 1995]. The KONUS instrument is controlled by the Astrophysics division and is a Russian instrument, thus not part of the Heliophysics data policies. The KONUS instrument does not receive any direct NASA funding through the project scientist, thus this section will be limited to just the instrument description and brief description of data products.

Each cylindrical NaI(Tl) crystal has a diameter of ∼127 mm and length of ∼76.2 mm. The crystals are housed in an aluminum case and the entrance aperture is covered by a beryllium (Be) window. The instrument has several measurement channels including two analog channels, A1 (∼10–750 keV) and A2 (∼0.2–10 MeV), four standard amplitude gamma ray channels, SG1 (∼10–50 keV) and SG2 (∼50–200 keV) and SG3 (∼200–750 keV) and SGZ (>10 MeV), and two enabled signal channels for controlling the operation of the pulse height analyzers, ES1 (∼10–750 keV) and ES2 (∼0.2–10 MeV). Nominally the burst mode can measure gamma rays covering ∼0.2–15 MeV at a cadence of $\gtrsim$2 ms with $\Delta E_\nu/E_\nu \gtrsim 5\%$ while the background mode covers ∼0.02–1.5 MeV at a cadence of $\gtrsim$3 s. The KONUS instrument was designed to measure GRBs and solar flares. Between November 1994 and mid-2019, it has measured $\gtrsim$2740 GRBs, $\gtrsim$1040 solar flares, ∼500 short GRBs, and ∼270 soft gamma repeaters (SGRs) [*Frederiks et al.*, 2019].

2.8 TGRS Instrument

The *Wind* TGRS instrument[28] has been powered off since January 2000, thus this section will be more brief than some other instrument descriptions. That is, this section will be a summary of the instrument papers [*Owens et al.*, 1991, 1995]. The instrument was designed to measure sources such as GRBs, bright galactic transient sources, the galactic center, the Crab Nebula, and solar flares.

The *Wind* TGRS instrument is a ∼215 cm^3 cylinder (∼6.7 cm diameter, ∼6.1 cm length) high purity n-type germanium (Ge) crystal with a 170° FOV FWFM[29]. The instrument measured photons with energies satisfying 25 keV $\lesssim E_\nu \lesssim$ 8.217 MeV and an energy resolution of ΔE_ν ∼ 3 keV at 1 MeV. The intrinsic time resolution is ∼62 μs but becomes ±1.5 ms after ground processing/calibration.

The instrument assembly is surrounded by a two-part radiative cooling system. A ∼30 mil (∼0.762 mm) beryllium-copper (BeCu) alloy passive-Sun-shield was included around the outside of the outer radiative cooler. Surrounding ∼90° of this Sun shield is a ∼13.5 mm thick molybdenum/lead (Mo/Pb), ∼1.5 mm of Mo and ∼12 mm of Pb, shield that acts as an occulter for ecliptic plane sources[30]. The outer radiative stage aperture is covered by fine ∼2 mil (∼0.0508 mm) BeCu wires to prevent stray fields due to spacecraft/instrument charging from interfering with onboard electric field measurements (i.e., WAVES). The outer stage was designed to operate at ∼164 K (∼ -109 °C). The inner radiator was designed to operate at ∼85 K (∼ -188 °C). Both radiators are constructed from Be and magnesium (Mg) to minimize weight and x-ray attenuation. The radiating surfaces of both the inner and outer stages, however, are constructed entirely of Be.

The instrument samples data in 8192 discrete energy channels (1 channel ≈ 1 keV). To reduce memory, the first 200 channels are read out as 500 count histograms. There is an event-by-event burst mode for enhancements above channel 200. These are digitized and time-tagged to ∼62.5 μs and stored directly in the onboard 2.75 Mbit burst memory buffer. The instrument also stores 128 sectored, 64 channel histograms (∼2.8° of spacecraft rotation for ∼3 s spin period). Finally, 1024 and 8192 channel histograms are accumulated over ∼3 and ∼24 minutes, respectively (accumulation times are commandable from ground), to determine background.

[28] An interesting note is that the surface finish of the WAVES z-antenna (spin axis) was specifically chosen to reduce the amount of reflected sunlight hitting the TGRS cooling unit. The antenna seams/joints were also oriented to be out of the TGRS FOV.

[29] Full Width Fiftieth Maximum ≃ 2.38 FWHM

[30] The Mo acts to passively shield fluorescent photons produced in the lead layer.

3 Ground Operations

Early in its mission, *Wind* and the other GGS spacecraft relied on a very capable and extensive science operations center, the Science Planning and Operations Facility (SPOF). The SPOF was responsible for the collecting, distribution and active archiving of all level zero (LZ) and ancillary data products. The SPOF also ran daily the instrument team provided data processing software to produce quick turnaround, publicly available data, termed Key Parameters (KPs). The SPOF also provided science planning and software maintenance services.

With the passage of time, and with reducing funding levels, the SPOF had to be turned off and most of its functions were passed on to the instrument teams and to a small operation, the *Polar-Wind-Geotail* (PWG) system, that continues to perform some LZ and KP functions (currently run by Robert M. Candey (Code 672)). The PWG system handles the active archiving of LZ and ancillary files and their distribution to the instrument teams and various active archives. The PWG system also performs the rapid KP data production for all instruments. It resides at Goddard with the project scientist team. The PWG system has been streamlined onto only two computers (a data server and a data processor, with hot spares) and is fully automated to eliminate the need for data technicians. This system also serves as the interface to the *Wind* Near-Real-Time (NRT) data stream, which is real-time processed data during the daily ∼2 hour long spacecraft telemetry contact times.

Wind ground operations take place at Goddard and have fully transitioned from the legacy *Polar-Wind-Geotail* system to Multi-Mission Operations Center (MMOC) that consolidates *Wind* operations with that of ACE. This transition became necessary with the decommissioning of *Polar* on April 30, 2008 and it included an upgrade of the outdated and costly to maintain hardware and software. *Wind* operations were moved to the MMOC on March 11, 2010 with the MMOC Operational Readiness Review held on March 30, 2010. The automated distribution and archiving of level zero files and production of KP files takes place at Goddard in the Science Directorate under the control of the project scientist. The two server (plus backup) system are periodically upgraded and maintained at modest cost.

For cost saving measures, the flight operations team reduced staffing by 1 FTE in November 2008 and modified shift schedules to reduce operational coverage from twelve to eight hours (reducing the need for overtime and shift differential). With the successful transition of *Wind* flight operations into the MMOC, the staffing levels have been reduced by operating the ACE and *Wind* missions with a combined team that also includes non-traditional flight operations skills (hardware/software maintenance, Flight Dynamics attitude analysis). Re-engineering/upgrading existing systems has improved the efficiency of implementing IT Security and hardware/software maintenance as well as system administration. Automation is being implemented with a unified approach to further increase efficiency (e.g., SWE electron instrument auto-recovery and WAVES recovery after latch ups).

The data recovery rate for *Wind* for the years 2017 through 2019 averaged ∼99.1%, ∼99.7%, and ∼98.5%, respectively. Between the recovery from the 2016 TUA anomaly and December 2019, the median daily data recovery rate was >99.8%. Most data losses have resulted from Deep Space Network (DSN) errors (i.e., hardware and software issues) or due to schedule conflicts with other spacecraft launches and/or emergencies.

The current operation of *Wind* requires one ∼2 hour DSN support every other day, though contacts occur more frequently sometimes. This allows the up-linking of the Stored Command Table (SCT) load and the playback of the Digital Tape Recorder (DTR). *Wind* also maintains NRT solar wind monitoring during these 2 hour contacts. The primary responsibility of the MMOC is spacecraft commanding, trend and anomaly analysis, DSN scheduling, the maintenance of *Wind*

NRT passes, providing orbit solutions, and LZ file generation for each instrument and spacecraft HK files.

3.1 Data Flow

All data from the spacecraft starts at the DSN. The NRT data is checked/corrected by a Reed-Solomon error code prior to being forwarded to the MMOC. The playback data Reed-Solomon code is not checked due to a failure of the encoder. The data is also saved at JPL. The real-time data arriving in the MMOC is forwarded on to PWG. Immediately following the pass, a KONUS LZ product is generated and delivered using the in-MMOC data. The data saved at JPL is forwarded, shortly after the pass, to the level-zero processing (LZP) system run by the FOT (current POC is Eric S. Smith (Code 444)). LZP organizes the received telemetry, corrects/flags errors where possible, and outputs a daily pair of files for each instrument and a single pair for housekeeping data. One of the files includes a day's worth of telemetry from the instrument while the other summarizes the types of errors encountered in processing that data. Additionally, a "quick look" file is generated immediately upon receipt of data (so shortly after each ground station contact), covering the first hour but otherwise identical to the daily products. All the products are sent to PWG.

The NRT telemetry goes through DSN to the MMOC, slightly converted and sent to leppwg VMS for decommutating and available as NRT streams to the instrument teams, and also through the KP programs streamed to:
https://pwg.gsfc.nasa.gov/windnrt/.
The NRT telemetry and tape recorder dumps are both sent as files from DSN to the MMOC for decommutating into instrument-specific records and processing into instrument quick look and daily LZ files on the LZP system and then sent on to PWGdata.gsfc.nasa.gov. DSN also sends the original telemetry files to PWGdata directly, where they are converted from the new DSN format to the old format and both formats are saved. PWGdata sends the daily instrument LZ files on to the VMS system for running the KP programs to make CDF files that are also collected on PWGdata and sent to SPDF CDAWeb for archiving and display at: https://cdaweb.gsfc.nasa.gov/.
The MMOC computes orbit and attitude files and sends them to PWGdata, where they are sent to the VMS system for conversion to full and daily CDF files. These are sent to SPDF for use in CDAWeb. The LZ files are available via FTPS on pwg.gsfc.nasa.gov, and there are scripts for automatically pulling new data in the software directory. Below are the data flow processes for each instrument team.

MFI: The fluxgate magnetometer LZ files are pulled from the PWG system by **PI Andriy Koval (University of Maryland, Baltimore County/Code 672)** in addition to spacecraft HK files, spacecraft spin phase files, spacecraft attitude files, and spacecraft orbit files. The KP data products for this instrument are generated by the PWG system almost immediately upon receiving them. The initial set of fully calibrated (with the exception of B_z offset, which is extrapolated) CDF files is generated and sent to SPDF as v03 files within ∼1–2 weeks. After the B_z offset is finalized, a new set of final fully calibrated CDF files is sent to SPDF as v04 files within about three weeks after measurement. Since the fully calibrated v04 files are produced close to real time, a set of v05 CDF files is generated once per year as final archival files to account for any possible late updates to the instrument LZ files, spacecraft HK files, spacecraft spin phase files, spacecraft attitude files, and spacecraft orbit files. Note that v05 files are almost always identical to v04 files, and v04 is a fully calibrated science quality data product.

SWE: The instrument PI is currently[31] **Bennett A. Maruca (University of Delaware)**.

[31] The paperwork to select a new SWE PI was submitted the NASA HQ in July 2020.

The KP data for this instrument are generated by the PWG system but the LZ files are pulled from the PWG system by **Michael Stevens (Harvard Smithsonian Center for Astrophysics SAO)** and then the ion Faraday Cup data is processed into CDF files and sent to SPDF for archival. This is particle data and so it relies upon properly calibrated magnetic field data from MFI, so the final versions of these data products are often delayed by ∼1–2 weeks from real time. The electron data for this instrument are also pulled from the PWG and processed by **Jan Merka (University of Maryland, Baltimore County/Code 672)** into CDF files which are sent off to SPDF for archival. Similar to the ion data, these are often delayed by a ∼1–2 weeks while waiting for the calibrated MFI data.

3DP: The instrument PI is currently **Stuart D. Bale (University of California, Berkeley SSL)**. The LZ files are manually pulled from the PWG system and CDF files are manually generated by **Peter Schroeder (University of California, Berkeley SSL)** then sent off to SPDF for archival. Similar to the SWE data, these are often delayed by ∼1–2 weeks while waiting for the calibrated MFI data.

SMS: The instrument PI is currently **Susan T. Lepri (University of Michigan, Ann Arbor)**. The KP data for this instrument are generated by the PWG system but the LZ files are automatically pulled from the PWG system by FTPS scripts. More automated scripts generate instrument health/status products, typically within a few hours of a DSN downlink. The higher level data products for the STICS instrument are processed manually by **Jim Raines (University of Michigan, Ann Arbor)** and then sent to SPDF for archival. SWICS is no longer operational and the MASS data products are kept at the instrument PI's institution.

EPACT: The instrument PI is currently **Ian G. Richardson (University of Maryland, College Park/Code 672)**. The LZ files are automatically transferred to another server at GSFC that produces ENC and HEX files by **Lawrence E. Brown (Johns Hopkins University APL)**. The ENC files are taken by **Donald V. Reames (University of Maryland, College Park)** and further processed for the LEMT instrument into physical units then sent along to **Lun-Chang Tan (University of Maryland, College Park)** who cleans up and calibrates the data before sending ASCII files to the SPDF for archival. The HEX files generated by **Lawrence E. Brown (Johns Hopkins University APL)** are automatically pulled by **Mihir I. Desai (Southwest Research Institute)** to generate calibrated STEP data products, which are then sent along to SPDF for archival. The IT instrument has been off since early in the mission and the APE data products are greatly reduced.

WAVES: The instrument American PI is currently **Keith Goetz (University of Minnesota, Twin Cities)** while the French PI is **Karine Issautier (Observatoire de Paris-Meudon)**. The LZ files are automatically transferred to another server at UMN by **Keith Goetz (University of Minnesota, Twin Cities)** and the radio data products are calibrated and posted on the instrument webpage in addition to being sent to SPDF for archival. The LZ files are also automatically pulled by Quynh Nhu Nguyen (Observatoire de Paris-Meudon) to their respective institutions for generation of calibrated data products. These are not yet archived at SPDF but progress in archiving the data generated by Keith Goetz (University of Minnesota, Twin Cities) has been slowly moving forward for several years.

KONUS: The instrument PI is currently **Dmitry Frederiks (Ioffe Institute, Laboratory for Experimental Astrophysics, St. Petersburg, Russia)**. The KONUS instrument is run by and was built by our Russian colleagues, therefore is not funded through NASA. However, the GCN uses KONUS data and the host machine receives the KONUS-only telemetry stream sent by the MMOC after receiving the raw data from JPL. The LZ files are automatically transferred to another server at GSFC by **Teresa B. Sheets (Code 587)** and data products are generated and stored on the GCN servers operated by the Astrophysics Division at GSFC. The data can be

retrieved from the GCN website at:
https://gcn.gsfc.nasa.gov.

4 Data Products

The bulk of the instrument data dissemination takes place through SPDF CDAWeb that also serves as the *Wind* Active Archive. To aid the user community, we also developed a *Wind* project webpage[32] that identifies the entry point for each instrument data environment and provides some degree of common documentation. The *Wind* project webpage includes an updated list of publications and a link to the *Wind* Wikipedia webpage[33] that we developed. Most of the *Wind* data products can also be searched, down to the parameter level, through CDAWeb providing rapid access to a wide range of events in the very long duration *Wind* data set. Next we detail the data product status of each *Wind* instrument.

As of August 15, 2024, there are ∼69 selectable data types with ∼1703 total data products (including OMNI data products) on SPDF CDAWeb. Below we will outline and describe these data products by instrument.

[32] https://wind.nasa.gov
[33] http://en.wikipedia.org/wiki/WIND_(spacecraft)

4.1 SWE Ions

Documentation: The SWE Faraday Cup (FC) sub-system was designed to measure solar wind thermal protons and positive ions. The physical sensor is completely described in the *Space Science Reviews* article *Ogilvie et al.* [1995]. This article was also reproduced in the Global Geospace Mission book and portions of it are available through the *Wind* project webpage[34]. The data production procedures are described by *Ogilvie et al.* [1995] with a much more detailed discussion in *Kasper* [2002]. Error analysis results are included in each FC data file, where systematic uncertainties of the measurements and calibration against other *Wind* instruments are discussed in *Kasper et al.* [2006]. All of this information and is available on the *Wind* project webpage.

Data Products: The PWG system, on receipt of the LZ data, immediately processes a KP data product for SWE/FC. This automated procedure uses a convected isotropic Maxwellian to fit to the reduced distribution functions collected by the FC. These ASCII data files (92 s resolution) are available to the public within 24 hours of the observations at CDAWeb[35]. While the KP products were originally designed as browse, quick look data, the quality proved to be so high that this data product became a frequently used science level data product of the FC sub-system.

A data production algorithm was developed that employs a bi-Maxwellian fit and obtains anisotropic temperatures for protons and a separate fit for alpha-particles. The resulting data product (designated wi_h1_swe on SPDF CDAWeb), also contains the simpler moment computations primarily to allow direct comparison with the ACE SWEPAM proton data. The whole mission (i.e., late 1994 – Present) has been reprocessed with this new algorithm and is available generally till 1–2 months behind real time as it requires the final calibrated MFI magnetic field data that needs several months to be computed. Finally, the reduced velocity distribution functions (designated wi_sw_ion_dist_swe_faraday) or VDFs for the two FCs were released as a data product for the entire mission in March 2014. The details and documention for these data products can be found *Wind* project webpage[36] and at CDAWeb[37].

Table 11: Publicly Available SWE Ion Data Products

Data Product	Cadence	Coverage	Format	Location
KP Protons wi_k0_swe wi_k0_swe_rtn[e]	92 s	1994/11/17–Present[c]	CDF	CDAWeb[a]
Bi-Maxwellian Fits wi_h1_swe wi_h1_swe_rtn	92 s	1995/01/01–Present[c]	CDF	CDAWeb
Reduced VDFs[d] wi_sw_ion_dist_swe_faraday	92 s	1994/11/17–Present[c]	CDF	CDAWeb

[a] https://cdaweb.gsfc.nasa.gov/; [b] ∼1–2 month lag;
[c] present minus the appropriate lag discussed in the text; [d] velocity distribution functions;
[e] same as above but in RTN coordinates

It is also possible to obtain special proton beam fits on request from Michael Stevens (e-mail: mstevenscfa.harvard.edu) at the Harvard Center for Astrophysics. These fits are specialized in that they only treat events where there is an extra proton beam, in addition to the usual proton solar wind core and associated alpha-particle beam. The occurrence rate of such events is low enough to

[34] https://wind.nasa.gov
[35] https://cdaweb.gsfc.nasa.gov/
[36] https://wind.nasa.gov
[37] https://cdaweb.gsfc.nasa.gov/

limit this data product on an event-by-event basis. However, the availability of such a product is very important as it allows for tests of ion/ion instabilities.

Finally, Bennett Maruca released an open-source Python GUI – funded by NASA ROSES grants – called *Janus* that allows users to interactively fit bi-Maxwellians for multiple (selectable) species to the reduced velocity distributions. The advantage of such software is that it can account for situations with multiple proton beams in addition to the alpha-particle population and even O^{6+}. The software and documentation can be found on GitHub[38].

The list of publicly available data products are shown in Table 11. All of the FC data products are archived at the SPDF active archive.

[38] https://github.com/JanusWind

4.2 SWE Electrons

Documentation: The SWE electron sub-system consists of two electrostatic analyzers, the vector spectrometer (VEIS) and the Strahl spectrometer. They were designed to measure the solar wind electron distribution function. The sensors are fully described by *Ogilvie et al.* [1995] and the instrument description portion of this paper can also be found at the *Wind* project webpage[39]. There is additional documentation found on the calibration software webpage[40].

Due to a high voltage power supply failure the last available data from the VEIS detector is May 31, 2001. Since the Strahl detector has very similar capabilities (though it was used in a different manner at the beginning of the mission), the spacecraft instrument and on-ground data processing software were rewritten to recover the electron observations originally supplied by VEIS. The SWE *Space Science Reviews* article has been updated with these modifications and is available at the *Wind* project page along with a technical description of the new ground software algorithms. Moreover, the headers of the CDF data files have extensive documentation for each data product.

Data Products: There are four SWE electron data products: (1) electron moments from density to heat flux; (2) pitch-angle distributions with 30 angle and 13 energy bins; (3) reduced/averaged pitch-angle distribution data products; and (4) strahl observations. Starting on Aug 16, 2002, all of these four data products are generated by the new production software based on the reprogrammed Strahl detector measurements. In addition, the electron "moments" are no longer the result of integral moment calculations but estimated from the fitting of a single kappa distribution function to both the core and halo components.

Table 12: Publicly Available SWE Electron Data Products

Data Product	Cadence	Coverage	Format	Location
VEIS Data Products				
Moments wi_h0_swe	6–12 s	1994/12/29–2001/05/31[b]	CDF	CDAWeb[a]
Pitch-angle wi_h4_swe	12 s	1994/11/30–2001/07/10[b]	CDF	CDAWeb
Avg. Pitch-angle wi_m2_swe	12 s	1994/12/28–2001/07/10[b]	CDF	CDAWeb
Strahl Data Products				
Strahl wi_strahl0_swe	12 s	1994/12/29–2001/05/30[b]	CDF	CDAWeb
New Moments wi_h5_swe	12-15 s	2002/08/16–Present[c]	CDF	CDAWeb
New Pitch-angle wi_h3_swe	12-15 s	2002/08/16–Present[c]	CDF	CDAWeb
New Avg. Pitch-angle wi_m0_swe	12-15 s	2002/08/16–Present[c]	CDF	CDAWeb

[a] https://cdaweb.gsfc.nasa.gov/; [b] range on August 15, 2024 [c] present minus the appropriate lag discussed in the text

The current availability of the SWE electron data products is summarized Table 12. The data products with ranges ending before 2020 are all discontinued due to the loss of VEIS and reconfiguration of the Strahl detector.

[39] https://wind.nasa.gov
[40] https://github.com/lynnbwilsoniii/Wind_Decom_Code

4.3 3DP

Documentation: The *Wind*/3DP instrument consists of six different sensors. There are two electron (EESA) and two ion (PESA) electrostatic analyzers (ESAs) covering energies from ∼5 eV to 30 keV and three arrays of double-ended solid state telescopes (SST) for electrons (SST Foil) and ions (SST Open) for energies ∼25–500 keV and ∼70–7000 keV, respectively. The ESAs measure the core solar wind and lower energy suprathermal particles while the SSTs are entirely focused on suprathermals. The instrument is fully described by *Lin et al.* [1995]. The instrument description portion of this paper is reproduced at the *Wind* project web site.

The ESAs produce much larger volumes of data than can be telemetered to ground, so they rely heavily upon onboard processing and burst modes. As a result a large number of 3DP data products were developed, some based on onboard processing and some generated on the ground. Some documentation of these data products exist at the 3DP instrument webpage[41] and more documentation/notes can be found on the project scientist's IDL software webpage[42]. Extensive 3DP documentation can be found on the *Wind* project web site.

Data Products: As with most *Wind* instruments, the 3DP team has provided a KP production software to be run automatically on the PWG system. This data product (wi_k0_3dp) contains electron and ion fluxes at seven energies for each particle and some basic moment computations and can be found at CDAWeb for the whole duration of the mission. The rest of the data products include: (1) onboard proton velocity moments (wi_pm_3dp) with 3s resolution; (2) omnidirectional fluxes for thermal electrons (wi_elsp_3dp and wi_ehsp_3dp) and ions (wi_plsp_3dp); (3) pitch-angle distributions for thermal electrons (wi_elpd_3dp and wi_ehpd_3dp) and ions (wi_plpd_3dp); (4) omnidirectional fluxes for suprathermal electrons (wi_sfsp_3dp) and ions (wi_sosp_3dp); (5) pitch-angle distributions for suprathermal electrons (wi_sfpd_3dp) and ions (wi_sopd_3dp); (6) onboard electron velocity moments (wi_em_3dp, not corrected for spacecraft potential); and (7) nonlinear fits of electron velocity distributions (wi_emfits_e0_3dp, corrected for spacecraft potential).

The publicly available data products are shown in Table 13.

The current onboard electron moments (wi_em_3dp) suffer from effects of spacecraft charging (i.e., photoelectron contamination). Recent efforts have led to the creation of a new data product of electron velocity moments (wi_emfits_e0_3dp) which have accounted for the spacecraft potential and calibrated against the upper hybrid line for total electron density. The new data product has been released to SPDF and distributed as CDF files for the first ∼10 years of the mission. It comprises electron velocity moments – from density to heat flux – derived from nonlinear fits of the entire velocity distribution covered by EESA Low and High (i.e., few eV to ∼30 keV) at variable time resolutions depending upon instrument mode (e.g., ∼3s resolution in burst mode).

The 3DP team is currently working on a higher level data product that separates the three solar wind electron components – core, halo, and strahl – to produce a new publicly available dataset. The dataset would be similar to the wi_emfits_e0_3dp data product but separate moments for each of the three electron components. The delayed release of this data product (i.e., relative to the wi_emfits_e0_3dp data product) is due to the complexities involved in re-calibrating the micro-channel plate efficiency and deadtime tables for both EESA Low and High in order to more accurately determine the true spacecraft potential. These calibrations do not significantly affect the total velocity moments but can be critical for accurate separation and characterization of the tenuous halo and strahl components.

Another database [*Wilson III et al.*, 2019a] of nonlinear fits to the electron VDFs can be found

[41] http://sprg.ssl.berkeley.edu/wind3dp/
[42] https://github.com/lynnbwilsoniii/wind_3dp_pros

Table 13: Publicly Available 3DP Data Products

Data Product	Cadence	Coverage	Format	Location
KP Data wi_k0_3dp	92 s	1994/11/01–Present[l]	CDF	CDAWeb[a]
Proton Moments[b] wi_pm_3dp	3 s	1994/11/15–Present[l]	CDF	CDAWeb, Berkeley[c]
EESA Low Spectra[d] wi_elsp_3dp	24-98 s	1994/11/15–Present[l]	CDF	CDAWeb, Berkeley
EESA High Spectra[d] wi_ehsp_3dp	24-98 s	1994/12/20–Present[l]	CDF	CDAWeb, Berkeley
PESA Low Spectra[d] wi_plsp_3dp	24 s	1994/11/15–Present[l]	CDF	CDAWeb, Berkeley
EESA Low PADs[k] wi_elpd_3dp	24-98 s	1994/11/15–Present[l]	CDF	CDAWeb, Berkeley
EESA High PADs[d] wi_ehpd_3dp	24-98 s	1994/12/20–Present[l]	CDF	CDAWeb, Berkeley
SST[e] Foil Spectra[f] wi_sfsp_3dp	12 s	1994/11/15–Present[l]	CDF	CDAWeb, Berkeley
SST Open Spectra[f] wi_sosp_3dp	12 s	1994/11/15–Present[l]	CDF	CDAWeb, Berkeley
SST Foil PADs wi_sfpd_3dp	12 s	1994/11/15–Present[l]	CDF	CDAWeb, Berkeley
SST Open PADs wi_sopd_3dp	12 s	1994/11/15–Present[l]	CDF	CDAWeb, Berkeley
Electron Moments[g] wi_em_3dp	3 s	1994/11/15–Present[l]	CDF	CDAWeb, Berkeley
Nonlinear Electron VDF Fits[h] wi_emfits_e0_3dp	3–98[i] s	1995/01/01–2004/12/31[j]	CDF	CDAWeb, Berkeley
Core/Halo/Strahl Fits[m]	3–98[i] s	1995/01/01–1998/12/31[j]	CDF	CDAWeb

[a] https://cdaweb.gsfc.nasa.gov/; [b] onboard proton moments; [c] http://sprg.ssl.berkeley.edu/wind3dp/;
[d] E = electron; P = proton; L = low energy; H = high energy; SP = omni directional fluxes; PD = pitch-angle; [e] SST = solid state telescope; [f] SF = foil (electrons); SO = open (protons);
[g] onboard electron moments; [h] electron velocity moments; [i] varies depending on instrument mode;
[j] range on August 15, 2024; [k] pitch-angle distribution; [l] present minus the appropriate lag discussed in the text; [m] velocity moments for core, halo, and strahl electrons

on Zenodo[43]. The database contains all the relevant fit results from a three-part study on the energy partition of electrons across 52 interplanetary shocks between February 26, 1995 and February 20, 2000 [*Wilson III et al.*, 2019b,c, 2020]. The EESA Low electron data were corrected for spacecraft potential and fit to the sum three model functions to separate the core, halo, and strahl components of the electron VDF.

Finally, a database of spacecraft floating electric potential determined from the EESA Low data [*Wilson III et al.*, 2023a] can be found on Zenodo[44]. The data spans from January 1, 2005 to January 1, 2022.

[43] https://zenodo.org/records/2875806
[44] https://zenodo.org/records/8364797

4.4 SMS

Documentation: The *Wind* SMS instrument suite is composed of three separate instruments: the SupraThermal Ion Composition Spectrometer (STICS); the high resolution mass spectrometer (MASS); and the Solar Wind Ion Composition Spectrometer (SWICS). STICS determines mass, mass per charge, and energy for ions in the energy range from ∼6–230 keV/e. MASS determines elemental and isotopic abundances from ∼0.5–12 keV/e. SWICS initially provided mass, charge, and energy for ions in the energy range of ∼0.5-30 keV/e, but it failed early in the mission and was turned off in May 2000, thus produces no data. MASS has been in a fixed voltage mode since 26 June 2009 due to a DPU latch-up, resulting in reduced science output. These instruments are fully described by *Gloeckler et al.* [1995]. The Instrument calibration is fully described by *Ghielmetti et al.* [1983] and in the PhD thesis of K. Chotoo both available on the *Wind* project page. Additional data release notes are also archived on the *Wind* project page.

Data Products: Until the failure of the SWICS instrument on May 27, 2000, combined SWICS and STICS KP files were generated that contain alpha particle information along with some carbon and oxygen abundances and temperatures. This data product is still publicly available from CDAWeb. The SWICS failure resulted in a significant effort to re-prioritize MASS and STICS. A new software system was developed which automates many data analysis functions previously done manually. The system first simultaneously assigns events to specific ion species, removing any overlap and using the statistical properties of the measurements to maximum advantage. It then uses these assigned events to construct phase space density distribution functions and corrects these for the effects of instrument efficiency and sampling geometry. Finally, it outputs these distribution functions, error estimates, and count rates for each ion along with many intermediate products that facilitate detailed analysis. The software can perform arbitrary time integrations of the data and can optionally use an inversion method to remove overlap among ions in the instrument measurement space.

Daily averages of the proton and alpha particle phase space density distribution functions for the whole mission is already publicly available through the *Wind* project webpage. In addition, hourly resolution STICS and MASS energy spectra for select days by request throughout the mission are available in digital and graphical formats from the University of Michigan page[45]. The publicly available data products are shown in Table 14.

The SMS team has recently released an enhanced STICS dataset for the entire mission that includes full 3D distributions at ∼3 minute time resolutions. The current datasets are shown in Table 14. The data separate times when the spacecraft is in the solar wind and magnetosphere, indicated in the data type names. These data are completely unique to *Wind* for this energy range. The data are found on SPDF as CDF files. The SMS team is also working to release data products from the SMS MASS detector for the entire mission. Note that the current data products are still some of the highest time resolution data for these energy ranges.

[45] http://solar-heliospheric.engin.umich.edu/mission_db/spectra.php?craft=2

Table 14: Publicly Available SMS Data Products

Data Product	Cadence	Coverage	Format	Location
KP SWICS+STICS wi_k0_sms	4 hr	1994/12/12–2000/05/27	CDF	CDAWeb[a]
Magnetosphere wi_l2-30min_sms-stics-afm-magnetosphere[b,d] wi_l2-30min_sms-stics-erpa-magnetosphere[c,d]	30 min	1995/08/01–2004/04/28	CDF	CDAWeb
Magnetosphere wi_l2_3min_sms-stics-nvt-magnetosphere[e,d] wi_l2-3min_sms-stics-vdf-magnetosphere[f,d]	3 min	1995/08/01–2004/04/28	CDF	CDAWeb
Solar Wind wi_l2-30min_sms-stics-afm-solarwind[b,d] wi_l2-30min_sms-stics-erpa-solarwind[c,d]	30 min	1995/01/01–2021/06/30[l]	CDF	CDAWeb
Solar Wind wi_l2_3min_sms-stics-nvt-solarwind[e,d] wi_l2-3min_sms-stics-vdf-solarwind[f,d]	3 min	1995/01/01–2021/06/30[l]	CDF	CDAWeb
STICS[g]	1 day	1995/01/01–2007/12/31	ASCII	*Wind* Project[h]
SWICS+MASS[i]	1 hr	Select Days	ASCII	UMichigan[j]
STICS[k]	1 day	2005–2007	ASCII	UMichigan

[a] https://cdaweb.gsfc.nasa.gov/; [b] angular flux map; [c] energy-resolved pitch-angle distributions;
[d] H^+, He^+, He^{2+}, O^+, O^{6+}, C^{5+}, and Fe^{10+}; [e] density, velocity, temperature moments;
[f] velocity distribution functions; [g] proton and alpha-particle distribution functions; [h] https://wind.nasa.gov;
[i] energy spectra; [j] http://solar-heliospheric.engin.umich.edu/mission_db/spectra.php?craft=2;
[k] omnidirectional proton and alpha-particle distribution functions;
[l] updated periodically to more closely match present dates

4.5 EPACT

Documentation: The Energetic Particles: Acceleration, Composition and Transport (EPACT) investigation consists of multiple telescopes including: the Low Energy Matrix Telescope (LEMT); SupraThermal Energetic Particle telescope (STEP); and ELectron-Isotope TElescope system (ELITE). ELITE is composed of two Alpha-Proton-Electron (APE) telescopes and an Isotope Telescope (IT). IT failed early in the mission and was turned off while APE only returns two energy channels of ∼5 and ∼20 MeV protons during enhanced periods. LEMT – covering energies in the 1-10 MeV/nuc range – and STEP – measuring ions heavier than protons in the 20 keV to ∼1 MeV/nuc range – still continue to provide valuable data. These instruments have been described by *von Rosenvinge et al.* [1995b]. The instrument portion of this paper is reproduced on the *Wind* project webpage[46]. The STEP data available on CDAWeb is used and described in more detail in *Filwett et al.* [2017] and *Filwett et al.* [2019]. Additional instrument information is also available on the *Wind* project webpage.

Data Products: Fluxes for a select number of ions (helium, oxygen, iron and combined CNO) in energy bins below 1 MeV/nuc and averaged over 92 seconds are publicly available for the whole mission in KP files at CDAWeb. However, the low count rates of heavy ions leads to a significant fraction of this data product being null. A systematic search for events with non-zero count rates was been undertaken, where the team identified 41 multi-day duration periods of intense particle events in the 1997–2006 time range. For these intervals, hourly omnidirectional intensity (OMN), ion sectored count (SEC), and first order ion anisotropy data were generated. These ASCII text files are publicly available at the *Wind* project webpage. The publicly available data products are shown in Table 15.

Hourly-averaged omnidirectional particles fluxes from LEMT of the *Wind*/EPACT instrument are available from OMNIWeb[47] and SPDF CDAWeb. The data cover the nearly entire mission from November 3, 1994 – June 30, 2020 and are updated every ∼3–6 months. The *Wind*/EPACT STEP data products are updated less regularly. The release delays are largely the result of the small teams each of which only have a small fraction of their time available for data processing. The LEMT data on CDAWeb include He, C, O, Ne, Si, and Fe in seven energy bins (six for Ne) from ∼2–11 MeV/nucleon. The APE-B data on CDAWeb include only one energy channel in the ∼18–22 MeV range for protons. The STEP data include H, He, CNO, and Fe in the ∼0.020–2.56 MeV/nucleon range in ∼6–10 energy bins. The hourly STEP data includes the extra NeS ion group.

Note that the hourly LEMT and APE-B and all STEP data currently available on CDAWeb will continue to be updated for the foreseeable future. The rest of the data in Table 15 will not.

[46] https://wind.nasa.gov
[47] https://omniweb.gsfc.nasa.gov

Table 15: Publicly Available EPACT Data Products

Data Product	Cadence	Coverage	Format	Location
KP fluxes[h] wi_k0_epa	92 s	1994/11/16–Present[l]	CDF	CDAWeb[a]
OMN[b]	1 hr	41 Events	ASCII	*Wind* Project[c]
SEC[d]	1 hr	41 Events	ASCII	*Wind* Project
Anisotropy	1 hr	39 Events	ASCII	*Wind* Project
LEMT[f] wi_l2-5min-sep_epact-lemt	5 min	1994/11/03–2014/09/06[g]	CDF	CDAWeb
LEMT[f] wi_l2-1hour-sep_epact-lemt	1 hr	1994/11/03–Present[l]	CDF	CDAWeb
APE-B[f] wi_l2-1hour-sep_epact-ape_b	1 hr	1994/11/03–Present[l]	CDF	CDAWeb
STEP df[h] wi_epact_step-differential-ion-flux-1hr	1 hr	1994/11/21–Present[l]	CDF	CDAWeb
STEP Sectored[i] H^+ wi_epact_step-directional-diff-h-flux-10min	10 min	1994/11/21–Present[l]	CDF	CDAWeb
STEP Sectored He^{2+} wi_epact_step-directional-diff-he-flux-10min	10 min	1994/11/21–Present[l]	CDF	CDAWeb
STEP Sectored Fe^{X+j} wi_epact_step-directional-diff-fe-flux-10min	10 min	1994/11/21–Present[l]	CDF	CDAWeb
STEP Sectored CNO^{X+k} wi_epact_step-directional-diff-cno-flux-10min	10 min	1994/11/21–Present[l]	CDF	CDAWeb

[a] https://cdaweb.gsfc.nasa.gov/; [b] omnidirectional fluxes; [c] https://wind.nasa.gov;
[d] sectored counts; [e] https://omniweb.gsfc.nasa.gov; [f] omnidirectional fluxes; [g] range as of August 15, 2024;
[h] differential, omnidirectional fluxes; [i] differential, sectored fluxes;
[j] STEP does not discrimiate charge states but the minimum is likely 2+ for heavy ions with these energies;
[k] STEP could separate C and O, in principle, but events with sufficient counting statistics are rare so the three ions are lumped together; [l] present minus the appropriate lag discussed in the text

4.6 MFI

Documentation: The *Wind* Magnetic Field Investigation (MFI) is composed of two fluxgate magnetometers located at ∼2/3 of the total length and at the end of a long boom. The instrument measures DC-coupled vector magnetic fields up to a time resolution of ∼22 or ∼11 vectors/sec depending on the telemetry mode of the spacecraft. The instrument is completely described in an article by *Lepping et al.* [1995]. The instrument description sections of this paper are reproduced at the *Wind* project webpage[48]. The calibration algorithms employed in generating the MFI data products are described in *Farrell et al.* [1995], *Kepko et al.* [1996], and *Leinweber et al.* [2008], available at the *Wind* Project webpage. Additional information involved in the removal of spin tone higher harmonics can be found in *Koval and Szabo* [2013].

Data Products: The MFI team generates 3-vector magnetic fields at multiple time resolutions (e.g., 92 ms, 3 s, 92 s, etc.) with varying calibration qualities depending on the data product. Within 24 hours of measurement, the 92-second KP data is publicly available at SPDF CDAWeb. Within ∼1–2 weeks the MFI team produces fully calibrated (with the exception of B_z offset, which is extrapolated) high-resolution (usually 92 ms) and standard (3 second, 1 minute, and 1 hour averages) data products (version 3). Roughly three weeks after measurement, the final B_z offset is determined with uncertainties now reduced to ∼0.1 nT (version 4). The final fully calibrated version 4 CDF files replace the version 3 files when uploaded to SPDF CDAWeb. The final archival data product (version 5), which is almost always identical to version 4 data product, is generated once per year to account for any possible late updates to the instrument LZ files, spacecraft HK files, spacecraft spin phase files, spacecraft attitude files, and spacecraft orbit files. All of these file versions have the exact same internal format. The publicly available data products are shown in Table 16.

Table 16: Publicly Available MFI Data Products

Data Product	Cadence	Coverage	Format	Location
KP MFI wi_k0_mfi wi_k1-rtn_mfi[f]	92 s	2010/09/01–Present[c]	CDF	CDAWeb[b]
Standard Product[e] wi_h0_mfi wi_h3-rtn_mfi[f]	3 s, 1 min, 1 hr	1994/11/16–Present[c]	CDF	CDAWeb
High Resolution wi_h2_mfi wi_h4-rtn_mfi[f]	∼11 or ∼22 sps[d]	1994/11/16–Present[c]	CDF	CDAWeb

[a] range as of August 15, 2024 [b] https://cdaweb.gsfc.nasa.gov/; [c] present minus the appropriate lag discussed in the text; [d] samples per second; [e] i.e., most commonly used; [f] same as above but in RTN coordinates

The highest sample rate data (i.e., ∼11 or ∼22 sps, depending on spacecraft location relative to Earth) is kept in a separate CDF file (wi_h2_mfi) from the lower rate data (wi_h0_mfi) at 3 s, 1 min., and 1 hour resolutions. This is partly due to file size differences, backwards compatibility (i.e., the ∼11 sps was never included in the original wi_h0_mfi files), and differences in calibration efforts (e.g., spin tones and other effects not present in wi_h0_mfi data).

[48] https://wind.nasa.gov

4.7 WAVES

Documentation: The instrument related sections of this document are reproduced at the *Wind* project webpage[49]. Some additional documentation exists also at the WAVES instrument webpage[50]. The content and format of the various WAVES data products are also described on the instrument webpage. See also the discussion in Section 2.3.

Data Products: As with most other *Wind* instruments, WAVES also produces a KP data product that is immediately publicly available at CDAWeb. The WAVES KP data contains 3-minute averages of the electric field intensities at 76 log-spaced frequencies and electron density estimates based on neural network determined electron plasma frequency values. The WAVES team produces 1 min resolution radio data, within ∼1 week of observation, as a frequency vs. time intensity product and distributes these data on both the instrument webpage and CDAWeb. The ∼7–10 second total electron density estimates from the upper hybrid line are also made available on CDAWeb.

The WAVES team also maintains a Type II/IV catalog on the instrument website and a similar list can be found at the CDAW Data Center[51] or through a link on the *Wind* project webpage. The publicly available data products are shown in Table 17.

Table 17: Publicly Available WAVES Data Products

Data Product	Cadence	Coverage	Format	Location
KP wi_k0_wav	3 min	1994/11/10–Present[j]	CDF	CDAWeb[a]
TNR[b], RAD1, RAD2[c] wi_h1_wav	1 min	1994/11/10–Present[j]	ASCII, IDL Save, CDF	CDAWeb, WAVES[d]
High Res. n_e[e] wi_h0_wav	7-20 s	1994/11/10–Present[j]	CDF	CDAWeb
Radio Plots	1 min	1994/11/10–Present[j]	PNG, PDF	WAVES
Dust Impacts[f] wi_l3-dustimpact_waves	N/A	1995/01/01–2023/09/01[g]	CDF	CDAWeb
TDSF[h]	N/A	1995/01/01–2022/09/16[g]	IDL Save	Zenodo[i]

[a] https://cdaweb.gsfc.nasa.gov/; [b] Thermal Noise Receiver; [c] Radio Receiver Band 1, 2;
[d] https://spdf.gsfc.nasa.gov/pub/data/stereo/documents/websites/solar-radio/wind/index.html;
[e] electron number density [cm^{-3}]; [f] dust impact database; [g] range as of August 15, 2024;
[h] TDS Fast waveform captures; [i] https://zenodo.org/records/10107360; [j] present minus the appropriate lag discussed in the text

The dust impact database was produced by David Malaspina (PI) and Lynn. B. Wilson III (Co-I) for the WAVES–TDSF waveform captures. The database is publicly available on CDAWeb in CDF file format. The dataset includes the date and time, orientation and location of the spacecraft, impact location on the spacecraft body, dust signal type, etc. The details of the dataset are described in *Malaspina and Wilson III* [2016] and very detailed metadata can be found in the CDF files on CDAWeb.

The TDSF data used to create the dust impact database were uploaded to Zenodo and documented [*Wilson III*, 2023] for archival at:
https://zenodo.org/records/10107360.

[49] https://wind.nasa.gov
[50] https://spdf.gsfc.nasa.gov/pub/data/stereo/documents/websites/solar-radio/wind/index.html
[51] https://cdaw.gsfc.nasa.gov/CME_list/radio/waves_type2.html

The intent is that a final distribution of both TDSF and TDSS data will be created and sent to SPDF CDAWeb for final archive in the future. Like many of the other instruments, the available time for the personnel involved is very minimal so progress is slow.

4.8 KONUS and TGRS

Documentation: The KONUS and TGRS γ-ray instruments are not maintained by heliophysics. Their data production and data distribution is completely handled by the astrophysics division. Description of the instruments and links to their data products can be found at:
https://heasarc.gsfc.nasa.gov/docs/heasarc/missions/wind.html; and
https://heasarc.gsfc.nasa.gov/w3browse/all/ipngrb.html; and
https://gcn.gsfc.nasa.gov.

5 Data Usage Summary Instructions

As discussed elsewhere herein, the majority of data products are available publicly through SPDF CDAWeb. All of these data can be plotted through the CDAWeb interface or using CDF-reading software. The majority of the data can be remotely retrieved and plotted using routines contained within the Space Physics Environment Data Analysis System (SPEDAS) software libraries [*Angelopoulos et al.*, 2019]. Additional software libraries for more specialized analysis of, for instance, the 3DP particle data that are not included with SPEDAS have been written and documented by *Wilson III* [2021], called UMN3DP for reference, and can be found at:
https://github.com/lynnbwilsoniii/wind_3dp_pros.
The project scientist has also made (as much as available for distribution) the lz file decommutation software publicly available [*Wilson III et al.*, 2021b] at:
https://github.com/lynnbwilsoniii/Wind_Decom_Code.

The following sections will outline which of the dozens of available data types are reliable for scientific investigations and outline some basic introductory steps for using the above software libraries.

5.1 Pre-calibrated Science Quality Data Sets

The *Wind* data user may ask which of the data products described in Section 4 are relevant or worthy of use in scientific analysis. The redundancy of certain measurements creates tremendous advantages to the experienced user but could result in confusion for the beginners. Therefore, we will discuss where to start and what to look for when examining each data set.

Note that unless otherwise specified in Section 4, all KP data products should be used for survey purposes only, i.e., do not rely upon KP data products for scientific investigations that require accurately calibrated data products.

5.1.1 Quasi-static Magnetic Fields

The quasi-static (i.e., DC-coupled) magnetic field is measured by MFI, which consists of two fluxgate magnetometers. There are two primary data products that should be used for science investigations, **wi_h0_mfi** and **wi_h2_mfi**. The latter provides high cadence (i.e., ∼11 or ∼22 sps depending on spacecraft location and date) magnetic field vectors in the GSE and GSM coordinate systems. The former provides the same coordinate basis vectors but at the cadences of 3 s, 1 min, and 1 hr. There is also spacecraft position information in the same coordinates at the same cadences within these CDF files. This is the most straight forward instrument and data product available. The magnetic fields also happen to be some of the most accurate and robust of all data products.

5.1.2 Number Density Calibration

First, note that the "upper hybrid line" (sometimes called the "plasma line") from **wi_h1_wav** should always be used as the standard against which all density calculations/measurements are made! The upper hybrid line is the most unambiguous measure of the total electron density, n_e (see Appendix 5.1.6 for symbol definitions), in any plasma where the magnetic field magnitude, B_o, can be well measured [e.g., *Meyer-Vernet and Perche*, 1989]. The reason being is that the upper hybrid frequency, f_{uh}, is given by:

$$f_{uh}{}^2 = f_{pe}{}^2 + f_{ce}{}^2 \tag{2}$$

where f_{ce} is the electron cyclotron frequency ($\sim 27.99249\ B_o$[nT]) and f_{pe} is the electron plasma frequency ($\sim 8978.66281\ n_e{}^{1/2}$[cm^{-3}]). Thus, one can see that f_{uh} only depends upon n_e and B_o. If an instrument measures f_{uh} directly through the observation of the upper hybrid line and a user combines that with measurements of B_o, the user can invert to calculate n_e. This is the most accurate method for measuring the total electron density in a plasma. Nearly all space environments accessible for in situ measurements will satisfy quasi-neutrality given by:

$$n_e = \sum_s Z_s n_s \tag{3}$$

where Z_s and n_s are the charge state and number density of ion species s (e.g., $s = p$ for protons). Therefore, both thermal electron and ion particle instruments can calibrate their measurements to satisfy Equation 3.

5.1.3 Thermal Particle Data

There are several instruments that measure the thermal part of the velocity distribution function (VDF) of both electrons and ions. Starting with the ions, the following instruments will be discussed: SWE and 3DP.

Ions: The ion instrument for the SWE instrument suite is a Faraday cup [*Kasper et al.*, 2006; *Ogilvie et al.*, 1995]. It measures incident ions over a typical energy range of ∼0.15–8.0 keV with a ∼6.5% energy resolution. The energies are controlled by deflector grids and the cups have a lower energy bound to avoid saturation. Thus, this instrument is only effective in the solar wind where the incident ion populations are cold, fast beams[52]. While the instrument is limited to a specific region of space, when in the solar wind, the *Wind* SWE data products are some of the most reliable and heavily used by the space plasma community. The data product that most users rely upon is **wi_h1_swe** from SPDF CDAWeb, which offers proton and alpha-particle velocity moments at ∼92 second cadence. Note that the thermal speeds calculated for this data product are the 1D rms thermal speeds, $w_{Ts,j}$ (see Appendix 5.1.6 for symbol definitions). This SWE data product also removes the aberration in the spacecraft frame bulk velocity measurement due to the orbit of Earth about the sun (i.e., the Y-GSE velocity component has has 29.78 km/s subtracted from the spacecraft frame measurement). The total ion density measured by SWE is generally within 10–15% of n_e estimated from f_{uh}, i.e., it is high quality data.

Thermal ion measurements from the 3DP instrument suite are taken from two detectors, PESA Low and PESA High. Most investigations only examine PESA Low as it is much easier to work with and it is calibrated. The PESA High data requires the user calibrate the data themselves and is only available through the UMN3DP IDL software libraries. Thus, the following will be limited to PESA Low data products. The PESA Low instrument has user-commandable energy-angle tables allowing it to sample the solar wind over energies of ∼0.1–10.0 keV (14 logarithmically spaced energy channels) with a ∼20% energy resolution and up to ∼5.6° angular resolution.

The most commonly used and most readily available data product for the user is **wi_pm_3dp** from SPDF CDAWeb[53], which offers proton and alpha-particle velocity moments at ∼3 second cadence[54]. These are velocity moments calculated onboard by the instrument. Note that the deadtime[55] and efficiency[56] calibration tables have not been updated since ∼August 2000. As a result, the user will find that the proton number density from **wi_pm_3dp** is systematically offset from that found in **wi_h1_swe** after 2000. The offset grows very slowly over time but even in February 2019, for example, the difference between the **wi_pm_3dp** and **wi_h1_swe** values of n_p is typically less than 20%, with the former being smaller.

Electrons: The available options for electron velocity moment data are from **wi_em_3dp** and **wi_h5_swe**. The data from **wi_em_3dp** are onboard electron velocity moments and do not account for the spacecraft potential, thus should not be used for science investigations beyond superficial surveys of interesting features in the time series. Similar to **wi_pm_3dp**, there is an on ground calculated velocity moment data product called **wi_elm2_3dp**. This data does attempt to

[52]Cold and fast here are relative terms which imply the thermal speed is much less than the bulk flow speed.

[53]Note similar data products are available from **wi_plsp_3dp** but at a much lower cadence and the data are often less accurate despite their being calculated on the ground. The primary reason for the reduced accuracy is these data are computed from VDFs taken from a reduced anode resolution mode relative to **wi_pm_3dp**.

[54]The cadence is actually based on the sun pulse from the sun sensor, thus the spin rate of the spacecraft. However, the spin cadence has been kept near ∼3 seconds for nearly the entire mission for science purposes as the instruments were designed for this rate.

[55]The time period when the detector is unable to measure incident particles due to the channel's discharge recovery time, preamp cycle rates, etc. [e.g., *Meeks and Siegel*, 2008].

[56]Here the efficiency refers to corrections to the optical geometric factor that becomes anode-specific during calibration [e.g., see *Bordoni*, 1971; *Paschmann and Daly*, 1998].

account for the spacecraft potential, but since *Wind* cannot directly measure this parameter, the value is numerically estimated. The numerical estimates tend to systematically over estimate the spacecraft potential which, in turn, results in smaller(larger) values of $n_e(T_e)$ than would be found with a proper estimate for the spacecraft potential. Thus, neither **wi_em_3dp** or **wi_elm2_3dp** should be used for rigorous science investigations.

The data from **wi_h5_swe** is much more reliable though it too shows a systematic offset in n_e from the true value inverted from f_{uh}. The value of n_e from **wi_h5_swe** is typically within 10% of the n_p value from **wi_pm_3dp**. Note that while the values of n_e and T_e from **wi_h5_swe** are reasonable, the user should not use the electron bulk flow velocities, $\mathbf{V}_e$, from these data types.

For electron data in the solar wind prior to December 31, 2004 should be taken from **wi_emfits_e0_3dp**, as these are computed from nonlinear fits of the electron VDFs accounting for a proper spacecraft potential estimate and calibrated to match n_e estimated from f_{uh}. Example use of this data product can be found in *Wilson III et al.* [2018, 2023b].

5.1.4 Suprathermal Particle Data

There are several instruments that measure the suprathermal part of the VDF of both electrons and ions. The electrons above ∼1 keV are measured independently (i.e., energy ranges start above the thermal range or $E_{min} \gtrsim 100$ eV) only by the EESA High and SST Foil detectors, which are part of the 3DP instrument suite. Suprathermal protons are measured by SMS STICS, EPACT APE and STEP, and 3DP PESA High and SST Open. For the ions, suprathermal is used generically as ions with kinetic energy larger than the typical thermal energy of protons in the proton core[57] rest frame.

Electrons: The publicly available, calibrated data products for suprathermal electron data from the SPDF CDAWeb are:

- **wi_ehsp_3dp** ∼150 eV to ∼28 keV[58]
- **wi_ehpd_3dp** ∼150 eV to ∼28 keV
- **wi_sfsp_3dp** ∼27 keV to ∼511 keV
- **wi_sfpd_3dp** ∼27 keV to ∼511 keV

Note that the EESA High detector has several "bad" (i.e., noisy) angle bins that are not removed during the creation of either **wi_ehsp_3dp** or **wi_ehpd_3dp**. Therefore, care should be taken when using those data[59]. The "bad" angle bins in the SST Foil data, however, are removed prior to generating the daily CDF files for SPDF CDAWeb.

Protons: The publicly available, calibrated data products for suprathermal proton data from the SPDF CDAWeb are:

- **wi_sosp_3dp** ∼70 keV to ∼6000 keV
- **wi_sopd_3dp** ∼70 keV to ∼6000 keV
- **wi_l2-hplus-3min_sms-stics-magnetosphere** ∼6 keV to ∼230 keV
- **wi_l2-hplus-3min_sms-stics-solarwind** ∼6 keV to ∼230 keV
- **wi_l2-1hour-sep_epact-ape_b** ∼18.9 MeV to ∼21.9 MeV
- **wi_epact_step-differential-ion-flux-1hr** ∼0.1 MeV to ∼2.5 MeV
- **wi_epact_step-directional-diff-h-flux-10min** ∼0.1 MeV to ∼2.5 MeV

Most of these data are available for the entire mission except for the magnetosphere-only SMS STICS data products, which stop in 2004 after *Wind* permanently moved to L1. Note that there are "bad" (i.e., noisy) angle bins associated with the SST Open data. These bins are removed in the **wi_sopd_3dp** data product but not in the **wi_sosp_3dp** data product. However, in the latter all angle bins are averaged together for each energy bin which should reduce the noise contributions to each energy bin.

Heavy Ions: The publicly available, calibrated data products for suprathermal proton data from the SPDF CDAWeb are:

- **wi_sosp_3dp** ∼70 keV to ∼6000 keV
- **wi_sopd_3dp** ∼70 keV to ∼6000 keV
- **wi_l2-heplus-3min_sms-stics-magnetosphere** ∼6 keV to ∼230 keV
- **wi_l2-heplus-3min_sms-stics-solarwind** ∼6 keV to ∼230 keV

[57] The distinction of core versus other populations is sometimes ambiguous in the literature. Here, core refers to the part of the VDF with the largest phase space density and thus, the largest number density of all the subpopulations. Therefore, if two peaks are observed in a 3D VDF, the peak with the larger phase space density for that species is considered the core while the lower peak would be labeled as a beam or secondary beam.

[58] These are the typical energy ranges for each of these data products observed but they can be changed by uploading different energy table commands.

[59] The software written by *Wilson III* [2021] can remove "bad" angle bins and there are example crib sheets illustrating how this can be done.

- **wi_epact_step-differential-ion-flux-1hr** ∼0.046 MeV/nucleon to ∼1.67 MeV/nucleon for He, ∼0.03 MeV/nucleon to ∼1.25 MeV/nucleon for CNO, ∼0.03 MeV/nucleon to ∼1.25 MeV/nucleon for NeS, and ∼0.02 MeV/nucleon to ∼1.18 MeV/nucleon for Fe
- **wi_epact_step-directional-diff-he-flux-10min** ∼0.03 MeV/nucleon to ∼1.67 MeV/nucleon for He
- **wi_epact_step-directional-diff-cno-flux-10min** ∼0.03 MeV/nucleon to ∼1.25 MeV/nucleon for CNO
- **wi_epact_step-directional-diff-fe-flux-10min** ∼0.02 MeV/nucleon to ∼1.18 MeV/nucleon for Fe

5.1.5 High Frequency Electromagnetic Fields

The *Wind* WAVES instrument measures electric and magnetic fields in two ways: as a remote radio receiver for spectrograms and as an in situ instrument for time series vector fields.

Remote Radio: The radio data can be found in the **wi_h1_wav** data type covering ∼4 kHz to ∼13.6 MHz at one minute resolution. The user can also retrieve the high cadence n_e estimated from the upper hybrid line from the **wi_h0_wav** data type at ∼7–20 second cadence. Note that this latter is computed using an automated neural network algorithm that can give spurious results during strong Type II or III radio burst events. In general, the thermal particle number densities should always be compared with the upper hybrid line from **wi_h1_wav** to ensure the values are reliable.

in situ: The WAVES instrument contains two more receivers that record high cadence electric and magnetic fields in time series form. These are the time domain sampler (TDS) receivers. There are two of them, one fast (TDSF) and one slow (TDSS). The TDSF data documented by *Wilson III* [2023] and found at:
https://zenodo.org/records/10107360.
The TDSS data is not yet publicly available as of August 15, 2024 but efforts are currently underway to provide a combined data product to SPDF CDAWeb that will contain both the TDSF and TDSS waveform captures for the entire mission.

The TDSF data contain evidence of micron-sized dust particles impacting the spacecraft, observed as electric field spikes/pulses. Because of the very large collecting area of the spacecraft bus compared to the usual targeted dust detectors [e.g., see the *Ulysses* dust experiment *Gruen et al.*, 1992], *Wind* has observed >100,000 dust impact events. These are archived in the *Wind* dust impact database at SPDF CDAWeb under **wi_l3-dustimpact_waves** and documented in *Malaspina and Wilson III* [2016].

5.1.6 3DP lz Data Analysis

The *Wind* 3DP level zero (lz) data files can be analyzed using the software written by *Wilson III* [2021]. Details on how to install and implement can be found the companion *Wind* CMAD document.

Definitions and Notation

This appendix lists the symbols/notation used throughout.

fundamental parameters

- $\varepsilon_o \equiv$ permittivity of free space
- $\mu_o \equiv$ permeability of free space
- $c \equiv$ speed of light in vacuum $[km\ s^{-1}] = (\varepsilon_o\ \mu_o)^{-1/2}$
- $k_B \equiv$ the Boltzmann constant $[J\ K^{-1}]$
- $e \equiv$ the fundamental charge $[C]$

plasma parameters

- $\mathbf{B}_o \equiv$ quasi-static magnetic field vector $[nT]$ with magnitude B_o
- $n_s \equiv$ the number density $[cm^{-3}]$ of species s
- $m_s \equiv$ the mass $[kg]$ of species s
- $Z_s \equiv$ the charge state of species s
- $q_s = Z_s\ e \equiv$ the charge $[C]$ of species s
- $\rho_m = \sum_s m_s n_s \equiv$ total mass density $[kgcm^{-3}]$
- $\gamma_s \equiv$ polytropic index or ratio of specific heats $[N/A]$ of species s
- $T_{s,j} \equiv$ the scalar temperature $[eV]$ of the jth component of species s, j = $\parallel$, $\perp$, or tot where $\parallel(\perp)$ is parallel(perpendicular) with respect to $\mathbf{B}_o$ (see Equation 4a)
- $P_{s,j} = n_s\ k_B\ T_{s,j} \equiv$ the partial thermal pressure $[eV\ cm^{-3}]$ of the jth component of species s
- $P_{t,j} = \sum_s\ P_{s,j} \equiv$ the total pressure $[eV\ cm^{-3}]$ of the jth component, summed over all species
- $V_{Ts,j} \equiv$ the most probable thermal speed $[km\ s^{-1}]$ of a one-dimensional velocity distribution (see Equation 4b)
- $w_{Ts,j} = V_{Ts,j}/\sqrt{2} \equiv$ the rms thermal speed $[km\ s^{-1}]$ of a one-dimensional velocity distribution
- $\Omega_{cs} = 2\ \pi f_{cs} \equiv$ the angular cyclotron frequency $[rad\ s^{-1}]$ (see Equation 4c)
- $\omega_{ps} = 2\ \pi f_{ps} \equiv$ the angular plasma frequency $[rad\ s^{-1}]$ (see Equation 4d)
- $\Omega_{lh} = 2\ \pi\sqrt{f_{ce}\ f_{ci}} \equiv$ the angular lower hybrid resonance frequency $[rad\ s^{-1}]$
- $\Omega_{uh} = 2\ \pi\sqrt{{f_{ce}}^2 + {f_{pe}}^2} \equiv$ the angular upper hybrid resonance frequency $[rad\ s^{-1}]$
- $\lambda_{De} \equiv$ the electron Debye length $[m]$ (see Equation 4e)
- $\rho_{cs} \equiv$ the thermal gyroradius $[km]$ (see Equation 4f)
- $\lambda_s \equiv$ the inertial length $[km]$ (see Equation 4g)
- $\beta_{s,j} \equiv$ the plasma beta [N/A] of the jth component of species s (see Equation 4h)
- $V_A \equiv$ the Alfvén speed $[km\ s^{-1}]$ (see Equation 4i)
- $C_s \equiv$ the sound or ion-acoustic sound speed $[km\ s^{-1}]$ (see Equation 4j)
- $V_f \equiv$ the fast mode speed $[km\ s^{-1}]$ (see Equation 4l)
- $R_E \equiv$ mean equatorial radius of Earth (~6378 km)
- $R_L \equiv$ mean equatorial radius of Earth's moon (~1737 km)
- $R_s \equiv$ mean solar radius (~695,700 km)

where multiple parameters are given in the following equations:

$$T_{s,tot} = \frac{1}{3}\left(T_{s,\parallel} + 2\ T_{s,\perp}\right) \tag{4a}$$

$$V_{Ts,j} = \sqrt{\frac{2\ k_B\ T_{s,j}}{m_s}} \tag{4b}$$

$$\Omega_{cs} = \frac{q_s\ B_o}{m_s} \tag{4c}$$

$$\omega_{ps} = \sqrt{\frac{n_s\ {q_s}^2}{\varepsilon_o\ m_s}} \tag{4d}$$

$$\lambda_{De} = \frac{V_{Te,tot}}{\sqrt{2}\ \omega_{pe}} = \sqrt{\frac{\varepsilon_o\ k_B\ T_{e,tot}}{n_e\ e^2}} \tag{4e}$$

$$\rho_{cs} = \frac{V_{Ts,tot}}{\Omega_{cs}} \tag{4f}$$

$$\lambda_s = \frac{c}{\omega_{ps}} \tag{4g}$$

$$\beta_{s,j} = \frac{2\mu_o n_s k_B T_{s,j}}{{B_o}^2} \tag{4h}$$

$$V_A = \frac{B_o}{\sqrt{\mu_o n_i M_i}} \tag{4i}$$

$${C_s}^2 = \frac{\partial P}{\partial \rho_m} = \frac{\sum_s \gamma_s P_s}{\rho_m} \tag{4j}$$

$$2{V_f}^2 = \left({C_s}^2 + {V_A}^2\right) \tag{4k}$$

$$+ \sqrt{({C_s}^2 - {V_A}^2)^2 + 4{C_s}^2{V_A}^2 \sin^2\theta_{Bn}} \tag{4l}$$

Acronyms and Initialisms

3D . . . . . three-dimensional

3DP . . . . . Three-Dimensional Plasma and Energetic Particle Investigation (*Wind*/3DP)

ACE . . . . . Advanced Composition Explorer

ADC . . . . . Analog-to-Digital-Converter

APE . . . . . Alpha-Proton-Electron telescope (part of *Wind* EPACT/ELITE)

ARTEMIS . . . . . Acceleration, Reconnection, Turbulence and Electrodynamics of the Moon's Interaction with the Sun

AU . . . . . Astronomical Unit

CAP . . . . . Command and Attitude Processor

CCMC . . . . . Coordinated Community Modeling Center

CDAWeb . . . . . Coordinated Data Analysis Web

CDF . . . . . Common Data Format

CMAD . . . . . Calibration and Measurement Algorithms Document

CME . . . . . Coronal Mass Ejection

DSN . . . . . Deep Space Network

DTR . . . . . Digital Tape Recorder

EESA . . . . . Electron Electrostatic Analyzer (*Wind*/3DP)

ELITE . . . . . Electron-Isotope Telescope system (*Wind*/EPACT)

EPACT . . . . . Energetic Particles: Acceleration, Composition, and Transport (APE-ELITE-IT-LEMT package on *Wind*)

ESA . . . . . ElectroStatic Analyzer

ESA (agency) . . . . . European Space Agency

FC . . . . . Faraday Cup (e.g., *Wind*/SWE)

FOT . . . . . Flight Operations Team

FOV . . . . . Field-of-View

FTE . . . . . Full Time Equivalent

FTP . . . . . File Transfer Protocol

FWFM . . . . . Full Width Fiftieth Maximum $\simeq$ 2.38 FWHM

FWHM . . . . . Full Width Half Maximum

GCN . . . . . Gamma-ray Coordinates Network

GeV . . . . . Giga-electron volt

GF . . . . . Giant Flare

GGS . . . . . Global Geospace Science

GLE . . . . . Ground-Level Events

GRB . . . . . Gamma Ray Burst

GSFC . . . . . Goddard Space Flight Center

GUI . . . . . Graphical User Interface

HDP . . . . . Heliophysics Data Portal

HET . . . . . High-Energy Telescope

HETE-2 . . . . . High Energy Transient Explorer-2

HGO . . . . . Heliophysics Great Observatory

HK . . . . . House Keeping

HSO . . . . . Heliophysics System Observatory

HTR . . . . . High Time Resolution

ICME . . . . . Interplanetary Coronal Mass Ejection

IMF . . . . . Interplanetary Magnetic Field

INTEGRAL . . . . . INTErnational Gamma-Ray Astrophysics Laboratory

IP . . . . . Interplanetary

IPD . . . . . Interplanetary Dust

IPM . . . . . Interplanetary Medium

IPN . . . . . Interplanetary GRB Network

ISD . . . . . Interstellar Dust

ISS . . . . . International Space Station

ISTP . . . . . International Solar-Terrestrial Physics

IT (detector) . . . . . Isotope Telescope (part of *Wind* EPACT/ELITE)

ITOS . . . . . Integrated Test and Operations System

keV . . . . . kilo-electron volt

KONUS . . . . . Gamma-Ray Spectrometer (*Wind*/KONUS)

KP . . . . . Key Parameter

LEMT . . . . . Low Energy Matrix Telescopes (*Wind*/EPACT)

LET . . . . . Low Energy Telescope

LWS . . . . . Living With a Star

LZ . . . . . Level Zero

LZP . . . . . Level Zero Processing

MAG . . . . . Magnetic Field Experiment

MASS . . . . . high-resolution MASS spectrometer (*Wind*/SMS)

MCP . . . . . MicroChannel Plate

MeV . . . . . Mega-electron volt

MFI . . . . . Magnetic Field Investigation (*Wind*/MFI)

MMOC . . . . . Multi-Mission Operations Center

NASA . . . . . National Aeronautics and Space Administration

NRT . . . . . Near-Real-Time telemetry stream

OMNI . . . . . dataset on CDAWeb

PDMP . . . . . Project Data Management Plan

PESA . . . . . Ion (Proton) ESA (*Wind*/3DP)

PHA . . . . . Pulse Height Analyzed

POC . . . . . Point of Contact

PWG . . . . . Polar-Wind-Geotail ground system

RAD1 . . . . . radio receiver band 1

RAD2 . . . . . radio receiver band 2

RTN . . . . . Radial-Tangential-Normal coordinate system

SC . . . . . Solar Cycle

SCT . . . . . Stored Command Table

SEP . . . . . Solar Energetic Particle

SEPT . . . . . Solar Electron and Proton Telescope

SEU . . . . . Single Event Upset

SEZ . . . . . Solar Exclusion Zone

SGR . . . . . Soft Gamma Repeater

SIS . . . . . Solar Isotope Spectrometer

SIT . . . . . Suprathermal Ion Telescope

SMS . . . . . Solar Wind and Suprathermal Ion Composition Experiment (SWICS-MASS-STICS package on *Wind*)

SPASE . . . . . Space Physics Archive Search and Extract

SPDF . . . . . Space Physics Data Facility

SPEDAS . . . . . Space Physics Environment Data Analysis System

sps . . . . . samples per second

SSD . . . . . Solid State Detector

SST . . . . . Solid-State (semi-conductor detector) Telescope (*Wind*/3DP)

STE . . . . . SupraThermal Electron instrument

STEP . . . . . SupraThermal Energetic Particle Telescope (*Wind*/EPACT)

STEREO . . . . . Solar-Terrestrial Relations Observatory

STICS . . . . . SupraThermal Ion Composition Spectrometer (*Wind*/SMS)

STP . . . . . Solar Terrestrial Probe

Strahl . . . . . electron strahl sensor of *Wind*/SWE

SWE . . . . . Solar Wind Experiment (*Wind*/SWE)

SWEA . . . . . Solar Wind Electron Analyzer

SWEPAM . . . . . Solar Wind Electron Proton Alpha Monitor (ACE)

SWICS . . . . . Solar Wind Ion Composition Spectrometer (*Wind*/SMS)

SWIMS . . . . . Solar Wind Ion Mass Spectrometer

TDS . . . . . Time Domain Sampler (*Wind*/WAVES)

TDSF . . . . . TDS Fast Receiver (*Wind*/WAVES)

TDSS . . . . . TDS Slow Receiver (*Wind*/WAVES)

TGRS . . . . . Transient Gamma-Ray Spectrometer (*Wind*/TGRS)

THEMIS . . . . . Time History of Events and Macroscale Interactions during Substorms

TNR . . . . . Thermal Noise Receiver (e.g., part of *Wind*/WAVES)

TOF . . . . . Time-Of-Flight

TUA . . . . . Tape Unit A

TUB . . . . . Tape Unit B

ULEIS . . . . . Ultra Low Energy Isotope Spectrometer

UV . . . . . Ultra Violet [light]

VAX . . . . . Virtual Address eXtension

VDF . . . . . Velocity Distribution Function

VEIS . . . . . Vector Ion-Electron Spectrometers (*Wind*/SWE)

VHO . . . . . Virtual Heliophysics Observatory

VMS . . . . . Virtual Memory System

WYE . . . . . Work Year Equivalent

References

Acuña, M. H., K. W. Ogilvie, D. N. Baker, S. A. Curtis, D. H. Fairfield, and W. H. Mish (1995), The Global Geospace Science Program and Its Investigations, *Space Sci. Rev.*, **71**(1), 5–21, 10.1007/BF00751323.

Angelopoulos, V., P. Cruce, A. Drozdov, E. W. Grimes, N. Hatzigeorgiu, D. A. King, D. Larson, J. W. Lewis, J. M. McTiernan, D. A. Roberts, C. L. Russell, T. Hori, Y. Kasahara, A. Kumamoto, A. Matsuoka, Y. Miyashita, Y. Miyoshi, I. Shinohara, M. Teramoto, J. B. Faden, A. J. Halford, M. McCarthy, R. M. Millan, J. G. Sample, D. M. Smith, L. A. Woodger, A. Masson, A. A. Narock, K. Asamura, T. F. Chang, C.-Y. Chiang, Y. Kazama, K. Keika, S. Matsuda, T. Segawa, K. Seki, M. Shoji, S. W. Y. Tam, N. Umemura, B.-J. Wang, S.-Y. Wang, R. Redmon, J. V. Rodriguez, H. J. Singer, J. Vandegriff, S. Abe, M. Nose, A. Shinbori, Y.-M. Tanaka, S. UeNo, L. Andersson, P. Dunn, C. Fowler, J. S. Halekas, T. Hara, Y. Harada, C. O. Lee, R. Lillis, D. L. Mitchell, M. R. Argall, K. Bromund, J. L. Burch, I. J. Cohen, M. Galloy, B. Giles, A. N. Jaynes, O. Le Contel, M. Oka, T. D. Phan, B. M. Walsh, J. Westlake, F. D. Wilder, S. D. Bale, R. Livi, M. Pulupa, P. Whittlesey, A. DeWolfe, B. Harter, E. Lucas, U. Auster, J. W. Bonnell, C. M. Cully, E. Donovan, R. E. Ergun, H. U. Frey, B. Jackel, A. Keiling, H. Korth, J. P. McFadden, Y. Nishimura, F. Plaschke, P. Robert, D. L. Turner, J. M. Weygand, R. M. Candey, R. C. Johnson, T. Kovalick, M. H. Liu, R. E. McGuire, A. Breneman, K. Kersten, and P. Schroeder (2019), The Space Physics Environment Data Analysis System (SPEDAS), *Space Sci. Rev.*, **215**, 9, 10.1007/s11214-018-0576-4.

Aptekar, R. L., D. D. Frederiks, S. V. Golenetskii, V. N. Ilynskii, E. P. Mazets, V. N. Panov, Z. J. Sokolova, M. M. Terekhov, L. O. Sheshin, T. L. Cline, and D. E. Stilwell (1995), Konus-W Gamma-Ray Burst Experiment for the GGS Wind Spacecraft, *Space Sci. Rev.*, **71**, 265–272, 10.1007/BF00751332.

Bordoni, F. (1971), Channel electron multiplier efficiency for 10-1000 eV electrons, *Nucl. Inst. & Meth.*, **97**, 405, 10.1016/0029-554X(71)90300-4.

Bougeret, J.-L., M. L. Kaiser, P. J. Kellogg, R. Manning, K. Goetz, S. J. Monson, N. Monge, L. Friel, C. A. Meetre, C. Perche, L. Sitruk, and S. Hoang (1995), Waves: The Radio and Plasma Wave Investigation on the Wind Spacecraft, *Space Sci. Rev.*, **71**, 231–263, 10.1007/BF00751331.

Chotoo, K. (1998), Measurements of H(+), He(2+), and He(+), in Corotating Interaction Regions at 1 AU, Ph.D. thesis, University of Maryland College Park.

Domingo, V., B. Fleck, and A. I. Poland (1995), The SOHO Mission: an Overview, *Solar Phys.*, **162**(1-2), 1–37, 10.1007/BF00733425.

Escoubet, C. P., R. Schmidt, and M. L. Goldstein (1997), Cluster - Science and Mission Overview, *Space Sci. Rev.*, **79**, 11–32, 10.1023/A:1004923124586.

Farrell, W. M., R. F. Thompson, R. P. Lepping, and J. B. Byrnes (1995), A method of calibrating magnetometers on a spinning spacecraft, *IEEE Trans. Mag.*, **31**, 966–972, 10.1109/20.364770.

Filwett, R. J., M. I. Desai, M. A. Dayeh, and T. W. Broiles (2017), Source Population and Acceleration Location of Suprathermal Heavy Ions in Corotating Interaction Regions, *Astrophys. J.*, **838**(1), 23, 10.3847/1538-4357/aa5ca9.

Filwett, R. J., M. I. Desai, R. W. Ebert, and M. A. Dayeh (2019), Spectral Properties and Abundances of Suprathermal Heavy Ions in Compression Regions near 1 au, *Astrophys. J.*, **876**(1), 88, 10.3847/1538-4357/ab12cf.

Franz, J. R., P. M. Kintner, and J. S. Pickett (1998), POLAR observations of coherent electric field structures, *Geophys. Res. Lett.*, **25**, 1277–1280, 10.1029/98GL50870.

Fränz, M., and D. Harper (2002), Heliospheric coordinate systems, *Planet. Space Sci.*, **50**, 217–233.

Frederiks, D., D. Svinkin, A. Tsvetkova, R. Aptekar, S. Golenetskii, A. Kozlova, A. Lysenko, and M. Ulanov (2019), GRB observations with Konus-WIND experiment, *Mem. Soc. Astron. Ital.*, **90**(1–2), arXiv:1907.00402.

Ghielmetti, A. G., H. Balsiger, R. Baenninger, P. Eberhardt, J. Geiss, and D. T. Young (1983), Calibration system for satellite and rocket-borne ion mass spectrometers in the energy range from 5 eV/charge to 100 keV/charge, *Rev. Sci. Inst.*, **54**, 425–436, 10.1063/1.1137411.

Gloeckler, G., H. Balsiger, A. Bürgi, P. Bochsler, L. A. Fisk, A. B. Galvin, J. Geiss, F. Gliem, D. C. Hamilton, T. E. Holzer, D. Hovestadt, F. M. Ipavich, E. Kirsch, R. A. Lundgren, K. W. Ogilvie, R. B. Sheldon, and B. Wilken (1995), The Solar Wind and Suprathermal Ion Composition Investigation on the Wind Spacecraft, *Space Sci. Rev.*, **71**, 79–124, 10.1007/BF00751327.

Gruen, E., H. Fechtig, J. Kissel, D. Linkert, D. Maas, J. A. M. McDonnell, G. E. Morfill, G. Schwehm, H. A. Zook, and R. H. Giese (1992), The ULYSSES dust experiment, *Astron. & Astrophys. Suppl.*, **92**, 411–423.

Gruesbeck, J. R. (2013), Exploring the Origin of Coronal Mass Ejection Plasma from In Situ Observations of Ionic Charge State Composition, Ph.D. thesis, University of Michigan, Ann Arbor, advisor: Susan T. Lepri.

Harten, R., and K. Clark (1995), The Design Features of the GGS Wind and Polar Spacecraft, *Space Sci. Rev.*, **71**, 23–40, 10.1007/BF00751324.

Hospodarsky, G. B. (1992), Search coil magnetometers for the ISTP *Polar* and *Wind* spacecraft, Master's thesis, University of Iowa, advisor: Donald A. Gurnett.

Ipavich, F. M., R. A. Lundgren, B. A. Lambird, and G. Gloeckler (1978), Measurements of pulse-height defect in Au–Si detectors for H, He, C, N, O, Ne, Ar, Kr from ≈2 to ≈ 400 keV/nucleon, *Nucl. Inst. & Meth.*, **154**(2), 291–294, 10.1016/0029-554X(78)90412-3.

Jackson, J. D. (1998), *Classical Electrodynamics, 3rd Edition*, John Wiley & Sons, Inc., New York, NY.

Kasper, J. C. (2002), Solar wind plasma: Kinetic properties and micro-instabilities, Ph.D. thesis, MASSACHUSETTS INSTITUTE OF TECHNOLOGY, advisor: Alan J. Lazarus.

Kasper, J. C., A. J. Lazarus, J. T. Steinberg, K. W. Ogilvie, and A. Szabo (2006), Physics-based tests to identify the accuracy of solar wind ion measurements: A case study with the Wind Faraday Cups, *J. Geophys. Res.*, **111**, 3105, 10.1029/2005JA011442.

Kepko, E. L., K. K. Khurana, M. G. Kivelson, R. C. Elphic, and C. T. Russell (1996), Accurate determination of magnetic field gradients from four point vector measurements. I. Use of natural constraints on vector data obtained from a single spinning spacecraft, *Trans. Mag.*, **32**(2), 377–385, 10.1109/20.486522.

Koval, A., and A. Szabo (2013), Magnetic field turbulence spectra observed by the Wind spacecraft, in *American Institute of Physics Conference Series*, *American Institute of Physics Conference Series*, vol. 1539, edited by G. P. Zank, J. Borovsky, R. Bruno, J. Cirtain, S. Cranmer, H. Elliott, J. Giacalone, W. Gonzalez, G. Li, E. Marsch, E. Moebius, N. Pogorelov, J. Spann, and O. Verkhoglyadova, pp. 211–214, 10.1063/1.4811025.

Leinweber, H. K., C. T. Russell, K. Torkar, T. L. Zhang, and V. Angelopoulos (2008), An advanced approach to finding magnetometer zero levels in the interplanetary magnetic field, *Measurement Sci. Tech.*, **19**(5), 055104, 10.1088/0957-0233/19/5/055104.

Lepping, R. P., M. H. Acũna, L. F. Burlaga, W. M. Farrell, J. A. Slavin, K. H. Schatten, F. Mariani, N. F. Ness, F. M. Neubauer, Y. C. Whang, J. B. Byrnes, R. S. Kennon, P. V. Panetta, J. Scheifele, and E. M. Worley (1995), The Wind Magnetic Field Investigation, *Space Sci. Rev.*, **71**, 207–229,

10.1007/BF00751330.

Lin, R. P., K. A. Anderson, S. Ashford, C. Carlson, D. Curtis, R. Ergun, D. Larson, J. McFadden, M. McCarthy, G. K. Parks, H. Rème, J. M. Bosqued, J. Coutelier, F. Cotin, C. D'Uston, K.-P. Wenzel, T. R. Sanderson, J. Henrion, J. C. Ronnet, and G. Paschmann (1995), A Three-Dimensional Plasma and Energetic Particle Investigation for the Wind Spacecraft, *Space Sci. Rev.*, **71**, 125–153, 10.1007/BF00751328.

Malaspina, D. M., and L. B. Wilson III (2016), A database of interplanetary and interstellar dust detected by the Wind spacecraft, *J. Geophys. Res.*, **121**, 9369–9377, 10.1002/2016JA023209.

Malaspina, D. M., M. Horanyi, A. Zaslavsky, K. Goetz, L. B. Wilson III, and K. Kersten (2014), Interplanetary and interstellar dust observed by the Wind/WAVES electric field instrument, *Geophys. Res. Lett.*, **41**, 266–272, 10.1002/2013GL058786.

Meeks, C., and P. B. Siegel (2008), Dead time correction via the time series, *Amer. J. Phys.*, **76**, 589–590, 10.1119/1.2870432.

Meyer-Vernet, N., and C. Perche (1989), Tool kit for antennae and thermal noise near the plasma frequency, *J. Geophys. Res.*, **94**, 2405–2415, 10.1029/JA094iA03p02405.

Nishida, A. (1994), The Geotail mission, *Geophys. Res. Lett.*, **21**(25), 2871–2873, 10.1029/94GL01223.

Ogilvie, K. W., and M. D. Desch (1997), The wind spacecraft and its early scientific results, *Adv. Space Res.*, **20**, 559–568, 10.1016/S0273-1177(97)00439-0.

Ogilvie, K. W., D. J. Chornay, R. J. Fritzenreiter, F. Hunsaker, J. Keller, J. Lobell, G. Miller, J. D. Scudder, E. C. Sittler, Jr., R. B. Torbert, D. Bodet, G. Needell, A. J. Lazarus, J. T. Steinberg, J. H. Tappan, A. Mavretic, and E. Gergin (1995), SWE, A Comprehensive Plasma Instrument for the Wind Spacecraft, *Space Sci. Rev.*, **71**, 55–77, 10.1007/BF00751326.

Owens, A., R. Baker, T. L. Cline, N. Gehrels, J. Jermakian, T. Nolan, R. Ramaty, G. Smith, D. E. Stilwell, and B. J. Teegarden (1991), The transient gamma-ray spectrometer, *IEEE Trans. Nucl. Sci.*, **38**, 559–567, 10.1109/23.289357.

Owens, A., R. Baker, T. L. Cline, N. Gehrels, J. Jermakian, T. Nolan, R. Ramaty, H. Seifert, D. A. Shephard, G. Smith, D. E. Stilwell, B. J. Teegarden, C. P. Cork, D. A. Landis, P. N. Luke, N. W. Madden, D. Malone, R. H. Pehl, H. Yaver, K. Hurley, S. Mathias, and A. H. Post, Jr. (1995), A High-Resolution GE Spectrometer for Gamma-Ray Burst Astronomy, *Space Sci. Rev.*, **71**, 273–296, 10.1007/BF00751333.

Paschmann, G., and P. W. Daly (1998), Analysis Methods for Multi-Spacecraft Data. ISSI Scientific Reports Series SR-001, ESA/ISSI, Vol. 1. ISBN 1608-280X, 1998, *ISSI Sci. Rep. Ser.*, **1**.

Paul, J. M. (1971), The rate of energy loss and intrinsic resolution of silicon detectors, *Nucl. Inst. & Meth.*, **94**(2), 275–283, 10.1016/0029-554X(71)90579-9.

Reames, D. V. (2017), *Solar Energetic Particles*, *Lecture Notes in Physics*, vol. 932, Springer International Publishing AG, 10.1007/978-3-319-50871-9.

Skyrme, D. J. (1967), The passage of charged particles through silicon, *Nucl. Inst. & Meth.*, **57**, 61–73, 10.1016/0029-554X(67)90498-3.

Stone, E. C., A. M. Frandsen, R. A. Mewaldt, E. R. Christian, D. Margolies, J. F. Ormes, and F. Snow (1998), The Advanced Composition Explorer, *Space Sci. Rev.*, **86**, 1–22, 10.1023/A:1005082526237.

von Rosenvinge, T. T., L. M. Barbier, J. Karsch, R. Liberman, M. P. Madden, T. Nolan, D. V. Reames, L. Ryan, S. Singh, H. Trexel, G. Winkert, G. M. Mason, D. C. Hamilton, and P. Walpole (1995a), The

Energetic Particles: Acceleration, Composition, and Transport (EPACT) investigation on the WIND spacecraft, *Space Sci. Rev.*, **71**, 155–206, 10.1007/BF00751329.

von Rosenvinge, T. T., L. M. Barbier, J. Karsch, R. Liberman, M. P. Madden, T. Nolan, D. V. Reames, L. Ryan, S. Singh, H. Trexel, G. Winkert, G. M. Mason, D. C. Hamilton, and P. Walpole (1995b), The Energetic Particles: Acceleration, Composition, and Transport (EPACT) investigation on the WIND spacecraft, *Space Sci. Rev.*, **71**, 155–206, 10.1007/BF00751329.

Whipple, E., and H. Lancaster (1995), International Coordination of Solar Terrestrial Science, *Space Sci. Rev.*, **71**(1-4), 41–54, 10.1007/BF00751325.

Wilson III, L. B. (2010), The microphysics of collisionless shocks, Ph.D. thesis, University of Minnesota *lynn.b.wilsoniii@gmail.com*, publication Number: AAT 3426498; ISBN: 9781124274577; Advisor: Cynthia Cattell.

Wilson III, L. B. (2021), Space plasma missions idl software library, 10.5281/zenodo.6141586.

Wilson III, L. B. (2023), *Wind* waves tdsf dataset, 10.5281/zenodo.10107360.

Wilson III, L. B., C. A. Cattell, P. J. Kellogg, K. Goetz, K. Kersten, J. C. Kasper, A. Szabo, and M. Wilber (2010), Large-amplitude electrostatic waves observed at a supercritical interplanetary shock, *J. Geophys. Res.*, **115**, A12104, 10.1029/2010JA015332.

Wilson III, L. B., A. Koval, A. Szabo, A. Breneman, C. A. Cattell, K. Goetz, P. J. Kellogg, K. Kersten, J. C. Kasper, B. A. Maruca, and M. Pulupa (2012), Observations of electromagnetic whistler precursors at supercritical interplanetary shocks, *Geophys. Res. Lett.*, **39**, L08109, 10.1029/2012GL051581.

Wilson III, L. B., A. Koval, A. Szabo, A. Breneman, C. A. Cattell, K. Goetz, P. J. Kellogg, K. Kersten, J. C. Kasper, B. A. Maruca, and M. Pulupa (2013), Electromagnetic waves and electron anisotropies downstream of supercritical interplanetary shocks, *J. Geophys. Res.*, **118**(1), 5–16, 10.1029/2012JA018167.

Wilson III, L. B., M. L. Stevens, J. C. Kasper, K. G. Klein, B. Maruca, S. D. Bale, T. A. Bowen, M. P. Pulupa, and C. S. Salem (2018), The Statistical Properties of Solar Wind Temperature Parameters Near 1 au, *Astrophys. J. Suppl.*, **236**(2), 41, 10.3847/1538-4365/aab71c.

Wilson III, L. B., L.-J. Chen, S. Wang, S. J. Schwartz, D. L. Turner, M. L. Stevens, J. C. Kasper, A. Osmane, D. Caprioli, S. D. Bale, M. P. Pulupa, C. S. Salem, and K. A. Goodrich (2019a), Supplement to: Electron energy partition across interplanetary shocks, 10.5281/zenodo.2875806.

Wilson III, L. B., L.-J. Chen, S. Wang, S. J. Schwartz, D. L. Turner, M. L. Stevens, J. C. Kasper, A. Osmane, D. Caprioli, S. D. Bale, M. P. Pulupa, C. S. Salem, and K. A. Goodrich (2019b), Electron energy partition across interplanetary shocks: I. Methodology and Data Product, *Astrophys. J. Suppl.*, **243**(8), 10.3847/1538-4365/ab22bd.

Wilson III, L. B., L.-J. Chen, S. Wang, S. J. Schwartz, D. L. Turner, M. L. Stevens, J. C. Kasper, A. Osmane, D. Caprioli, S. D. Bale, M. P. Pulupa, C. S. Salem, and K. A. Goodrich (2019c), Electron energy partition across interplanetary shocks: II. Statistics, *Astrophys. J. Suppl.*, **245**(24), 10.3847/1538-4365/ab5445.

Wilson III, L. B., L.-J. Chen, S. Wang, S. J. Schwartz, D. L. Turner, M. L. Stevens, J. C. Kasper, A. Osmane, D. Caprioli, S. D. Bale, M. P. Pulupa, C. S. Salem, and K. A. Goodrich (2020), Electron energy partition across interplanetary shocks: III. Analysis, *Astrophys. J.*, **893**(22), 10.3847/1538-4357/ab7d39.

Wilson III, L. B., A. L. Brosius, N. Gopalswamy, T. Nieves-Chinchilla, A. Szabo, K. Hurley, T. Phan, J. Kasper, N. Lugaz, I. G. Richardson, C. H. K. Chen, D. Verscharen, R. T. Wicks, and J. M. TenBarge (2021a), A Quarter Century of *Wind* Spacecraft Discoveries, *Rev. Geophys.*, **59**(2), e2020RG000,714, 10.1029/2020RG000714.

Wilson III, L. B., C. S. Salem, and J. W. Bonnell (2023a), Spacecraft floating potential measurements for the *Wind* spacecraft, *Astrophys. J. Suppl.*, **269**(52), 10, 10.3847/1538-4365/ad0633.

Wilson III, L. B., M. L. Stevens, J. C. Kasper, K. G. Klein, B. Maruca, S. D. Bale, T. A. Bowen, M. P. Pulupa, and C. S. Salem (2023b), Erratum: "The Statistical Properties of Solar Wind Temperature Parameters Near 1 au", *Astrophys. J. Suppl.*, **269**(62), 12, 10.3847/1538-4365/ad07de.

Wilson III, L. B., et al. (2021b), *Wind* lz calibration and decommutation software, 10.5281/zenodo.4451304.